



저작자표시-비영리-변경금지 2.0 대한민국

이용자는 아래의 조건을 따르는 경우에 한하여 자유롭게

- 이 저작물을 복제, 배포, 전송, 전시, 공연 및 방송할 수 있습니다.

다음과 같은 조건을 따라야 합니다:



저작자표시. 귀하는 원저작자를 표시하여야 합니다.



비영리. 귀하는 이 저작물을 영리 목적으로 이용할 수 없습니다.



변경금지. 귀하는 이 저작물을 개작, 변형 또는 가공할 수 없습니다.

- 귀하는, 이 저작물의 재이용이나 배포의 경우, 이 저작물에 적용된 이용허락조건을 명확하게 나타내어야 합니다.
- 저작권자로부터 별도의 허가를 받으면 이러한 조건들은 적용되지 않습니다.

저작권법에 따른 이용자의 권리는 위의 내용에 의하여 영향을 받지 않습니다.

이것은 [이용허락규약\(Legal Code\)](#)을 이해하기 쉽게 요약한 것입니다.

[Disclaimer](#)

Thesis for the *Master of Science*

Torque Distribution based on Real-Time Weighting Matrix
Optimization between AUV and Underwater Manipulator

Ye Cheol MOON

Graduate School of Hanyang University

August 2020

Thesis for the *Master of Science*

Torque Distribution based on Real-Time Weighting Matrix
Optimization between AUV and Underwater Manipulator

Thesis Supervisor: Tae Won SEO

A Thesis submitted to the graduate school of
Hanyang University in partial fulfillment of the requirements
for the degree of *Master of Science*

Ye Cheol MOON

August 2020

Department of Mechanical Convergence Engineering
Graduate School of Hanyang University

This thesis, written by Ye Cheol Moon,
has been approved as a thesis for the Master of Science

August 2020

Committee Chairman: Wang Wei  (Signature)

Committee member: Taewon Seo  (Signature)

Committee member: Sangrok Jin  (Signature)

Committee member: _____ (Signature)

Committee member: _____ (Signature)

Graduate School of Hanyang University

Table of contents

Chapter 1. Introduction	1
Section 1 Research background	1
Section 1.1 The history of underwater robot research	1
Section 1.2 Underwater manipulator	3
Section 2 Previous research	4
Section 3 Research purpose	7
Chapter 2 Foundation of AURORA and manipulators	8
Section 1 AUV - Manipulator overall structure	8
Section 2 Underwater manipulator friction compensation	1 6
Section 3 Underwater manipulator analysis and control	1 7
Chapter 3 Real-time torque distribution algorithm	2 2
Section 1 Taguchi method	2 2
Section 2 Real-time Torque Squared Sum Minimization Algorithm	2 5
Chapter 4 Experiment and results analysis	3 1
Section 1 Experiment setup	3 1
Section 2 Results of Previous Study Using Weighted Matrix	3 2
Chapter 5 Conclusion	4 3
Reference	4 4
Appendix	4 6
국문 요지	4 7

List of Figure

Fig. 1 Annual refined petroleum products consumption.....	1
Fig. 2 CURV (Cable-Controlled Underwater Recovery Vehicle) I and III	2
Fig. 3 Various manipulators (Kraft Raptor, Schilling Titan 4, Cybernetix Maestro, Hydro-lek 40500R, Eca robotics 7E, Ansaldo Maris 7080, Graal Tech UMA) [7].....	3
Fig. 4 Actual hovering and terminal operation of TTURT	5
Fig. 5 AURORA hovering control	5
Fig. 6 Valve operation of UVMS	6
Fig. 7 History of underwater robot project.....	6
Fig. 8 The entire main body and manipulator used in this study.....	8
Fig. 9 AURORA Parts Structure.....	9
Fig. 10 AURORA appearance and structure.....	9
Fig. 11 AURORA drive-related parts.....	10
Fig. 12 Appearance and structure of thruster T200 used in aurora.....	10
Fig. 13 Tilting motor EC-i 40.....	11
Fig. 14 Camera box.....	12
Fig. 15 Signal map of the robotic platform. [13]	12
Fig. 16 Structure and exploded view of the manipulator joint	13
Fig. 17 Assembled Clamping Manipulator.....	14
Fig. 18 Manipulator joint casing.....	14
Fig. 19 Rotary seals that block leakage in the direction of the drive shaft, the motor driver and wires inside the drive shaft and casing	15
Fig. 20 Attached buoyancy material	16

Fig. 21 Dahl model friction graph [15]	1 7
Fig. 22 Manipulator Control Flowchart	1 7
Fig. 23 AURORA – Manipulator Diagram	1 8
Fig. 24 Valve dimensions and rotation angle.....	1 8
Fig. 25 Valve rotation speed over time [13]	1 9
Fig. 26 Linear graph used for OA construction	2 4
Fig. 27 Real-time Taguchi Torque Squared Minimization Algorithm Flowchart.....	2 6
Fig. 28 Problem formulation of a real-time torque sum-of-squares minimization algorithm.....	2 7
Fig. 29 Type of S/N Ratio and design variable aspects after that	2 9
Fig. 30 Test bench and valve structures	3 2
Fig. 32 AURORA – UVMS in actual experiment	3 2
Fig. 34 The error value for the valve angle and actual rotation angle	3 3
Fig. 35 Torque change of working manipulator joint W1~3 over time	3 4
Fig. 36 Torque change of working manipulator joint C1~2 over time	3 5
Fig. 37 Changes in the force and rotational torque of the AURORA body over time	3 6
Fig. 38 Comparison of the maximum torque applied to the joint during valve operation.....	3 7
Fig. 39 Change of maximum value among manipulator joints over time.....	3 8
Fig. 40 Change over time of weighted matrix elements $w_1 \sim w_3$	3 9
Fig. 41 Change over time of weighted matrix elements $w_4 \sim w_6$	4 0
Fig. 42 Change over time of weighted matrix elements $w_7 \sim w_9$	4 1
Fig. 43 Change over time of weighted matrix elements $w_{10} \sim w_{11}$	4 2

List of Table

Table 1 Comparison of each underwater robot research project	7
Table 2 T200 Specification.....	1 0
Table 3 EC-I 40 specification	1 1
Table 4 Thrust, tilting motor modeling [13]	1 1
Table 5 Electric components of AURORA	1 2
Table 6 Electric components of the dual-arm manipulator. [11]	1 5
Table 7 Buoyancy calculation result by manipulator part.....	1 6
Table 8 Taguchi method procedure [20].....	2 3
Table 9 S/N Ratio according to the objective function value [21].....	2 5
Table 10 Orthogonal array for weight calculation	2 8
Table 11 Set initial value and initial stage of weighting matrix	3 0
Table 12 Error value after operation in each case.....	3 3
Table 13 Comparison of the average of the real-time Taguchi weighting matrix determination algorithm and the maximum torque of each joint in the case of a fixed constant	3 7
Table 14 Comparison difference of the maximum force and torque applied to the robot body in the case of the average and fixed constants of a real-time Taguchi weighting matrix determination algorithm.....	3 8
Table 15 Torque increase/decrease value compared to fixed constant when the result of the algorithm is highest, worst, or average.....	3 8

ABSTRACT

Torque Distribution based on Real-Time Weighting Matrix Optimization between AUV and Underwater Manipulator

On the seabed, there are resources with various possibilities of utilization, and various underwater robot technologies have been developed to utilize them. Among them, underwater valve control technology that is frequently used in oil and gas mining has also been studied. In the previous study, a study was conducted to lower the torque of the joint by distributing the joint burden to the robot body during the valve operation.

However, this study did not discuss ways to further reduce joint torque. In this study, based on the Taguchi method, we proposed a new algorithm that can reduce the torque of the joint in changing environment by determining the weighting matrix based on sensor values in real time.

In order to prove the effectiveness of this algorithm, iterative experiments of the algorithm of this study and the case of fixed weighted matrices were performed in a real water tank. Therefore, the effectiveness of this algorithm was proved by observing that the maximum torque of the manipulator joint is lowered by 35~55% than the valve work with the existing fixed weight matrix.

Chapter 1. Introduction

Section 1 Research background

Section 1.1 The history of underwater robot research

Consumption of oil resources continued to increase from 57236 Mb/d in 1973 to 98764 Mb/d in 2017. [1]

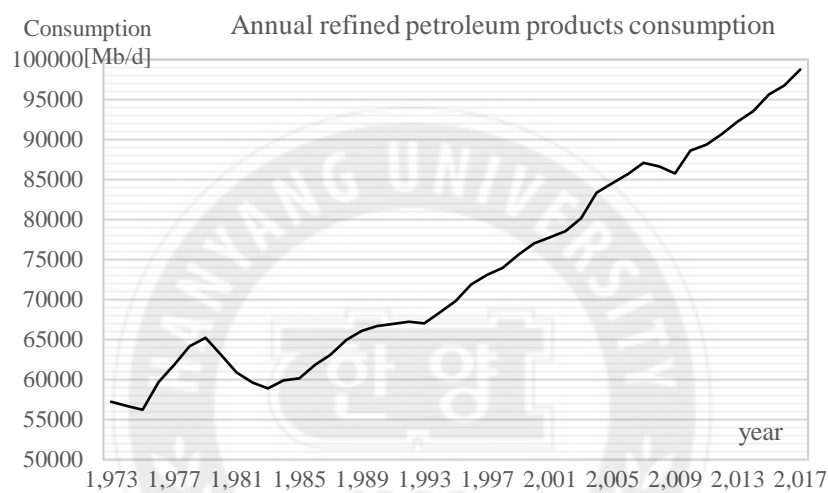


Fig. 1 Annual refined petroleum products consumption

As demand for oil resources increased, interest in oil resources buried on the seabed increased. However, it was only in 1960 that actual attempts were made because of the high level of science and technology required for submarine exploration and work. In 1960s, the United States Navy announced the first underwater navigation robot called the CURV (Cable-Controlled Underwater Recovery Vehicle), which established the basic form of the underwater robot. Later, gas and oil industries also began to study underwater exploration technology for abundant resources in the seabed. [2] Underwater robots have been developed not only for simple exploration, but also for carrying out various activities in the water, such as underwater plant construction. [3]

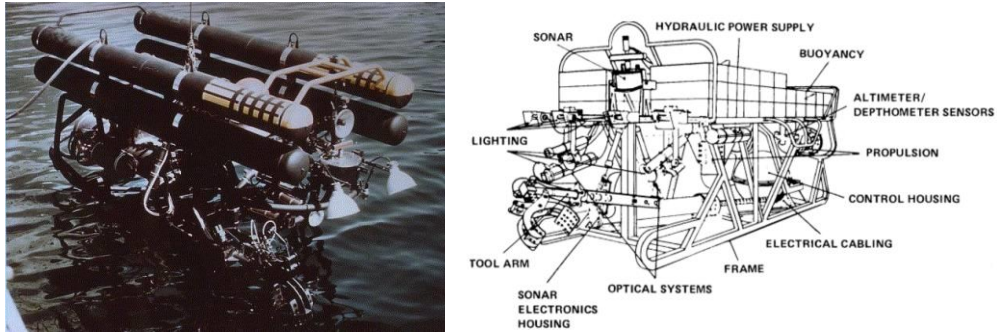


Fig. 2 CURV (Cable-Controlled Underwater Recovery Vehicle) I and III

These underwater robots have been driven by people manually, but mainly focused on the technology that allows the robots to collect and control information on their own without boarding. This is called Unmanned Underwater Vehicle (UUV), and among these UUVs, it is largely divided into two categories: Remotely Operated Vehicle (ROV) and Autonomous Unmanned Vehicle (AUV). [4] ROV means that the robot is manually controlled by an external controller using a camera attached to the robot while the robot is undersea. AUV is a form in which the robot autonomously controls its own motion by checking the state of the robot with a sensing device. Previously, a lot of ROVs were mainstream because they are controlled by a person, so do not require advanced control technology. [5] However, there was a limit to the operation because the operator outside water could not immediately check the condition of the robot on the seabed. Therefore, AUV technology that enables robots to quickly react automatically instead of manually operating them has also been studied. [6]

Section 1.2 Underwater manipulator



Fig. 3 Various manipulators (Kraft Raptor, Schilling Titan 4, Cybertetix Maestro, Hydro-lek 40500R, Eca robotics 7E, Ansaldo Maris 7080, Graal Tech UMA) [7]

In addition to observing underwater situations by using ROVs, the underwater manipulators have also been studied to control underwater situations. [7] Because one of the main goal of underwater robots is the exploration and mining of submarine resources, technologies used in oil and gas mining have also become major research areas. [2] Among them, underwater valve control operations that control the flow of fluid resources have also been studied. The one of the main topic of underwater valve operation research is reducing torque applied to the joints. Torque reduction methods include distributing torque to a pair of manipulators [8] and reducing the burden by clamping a surrounding structures. [9] Furthermore, torque reduction studies have been made by operating the propulsion of the main body to reduce the torque of the manipulator. [10] In the case of an underwater robot, various forces can be applied in various directions through a thruster, which makes it easier to distribute the force to the main body than a robot on the ground. In the previous study [11], methods for lowering the torque of the valve operation of the underwater manipulator were applied comprehensively. And as a result, it showed an effect of sufficiently reducing the torque. However, we did not consider how the distribution could lower the manipulator torque. Torque distribution between the manipulator and the robot body was performed using a weighting matrix in the control process. It has the advantage that the operator can more intuitively distribute the thruster and joint torque through the element determination of the matrix. However, no research

has been conducted on how to determine the weighting matrix focused on underwater manipulator, not the normal situation on the ground. Only the optimization theory, such as local optimization and global optimization using a genetic network, was used in the control. It was not specific to underwater manipulators, therefore limitations existed. In general, optimization techniques take a long time, so optimization is performed in advance and the results are applied to the work. It is difficult to adapt to various underwater conditions to use only optimization performed before operation. It is because there are many complex errors that are difficult to assume in advance, such as disturbance, obstacles, and clamping errors in underwater situations. Therefore, the need for real-time torque distribution that can be used in a variety of changing underwater situations has emerged. So, in this study, we are going to study on real-time torque distribution that can adapt to changes in the underwater environment of a parallel underwater manipulator and AUV.

Section 2 Previous research

This study has been established based on previous studies. In 2014, the research of the AUV platform equipped with four tilt thrusters and be attached to various terminals in the water was conducted first. It was TTURT (Tilting Thruster Underwater Robot) project [12].

In the TTURT, one motor was connected to the tilting devices of two thrusters through a bevel gear. It was only possible to control the tilt angle simultaneously left and right thruster. The angle was also controllable in software only at a right angle of 90 degrees. (0 degrees, 90 degrees, 180 degrees, and 270 degrees) Specifically, TTURT could maintain the current position and angle within a limited degree of freedom using the switching control. Based on this robot, the improvement project began. By changing the thruster drive system of the TTURT, the thrust force is also improved. In addition, the control system is changed from switching control for vertical tilting thruster to control for a free tilting angle. In

addition, one motor is connected to one thruster tilt device, so it is possible to control from different angles to the left and right. As a result, it is possible to control more positions and angles than previous studies based on increased degrees of freedom. It can be said that the robot and the method of control have been completely changed from the previous robot. To distinguish this, the robot was renamed to AURORA (An Underwater ROBot with tilting thrusters for Redundant Actuation). [13]

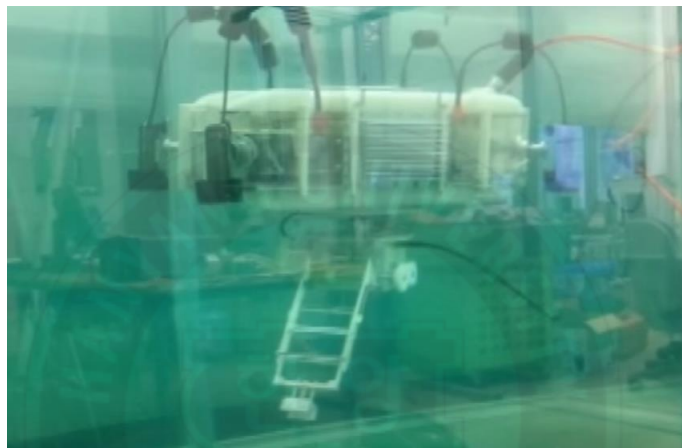


Fig. 4 Actual hovering and terminal operation of TTURT

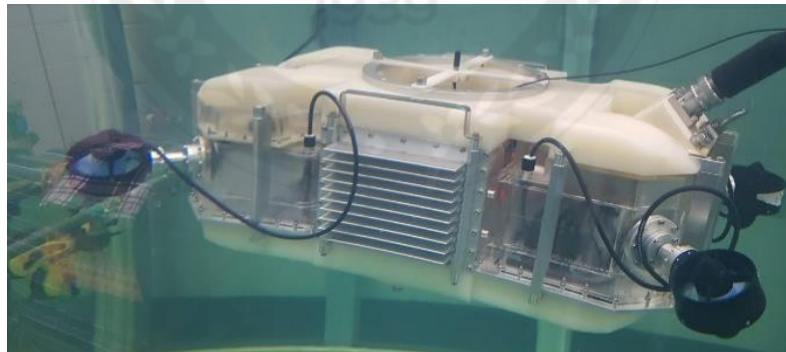


Fig. 5 AURORA hovering control

And before the robot changed to AURORA, a new manipulator was developed to perform valve turning tasks for TTURT. Generally, the manipulator system used with the AUV is called the UVMS (Underwater Vehicle Manipulator System). manipulator is designed to carry out valve work that is frequently used in industrial sites. It consists of two pairs of top and bottom. Algorithm of valve

operation with less torque load was studied through distribution of torque of this manipulator and thrust force of TTURT. [11]

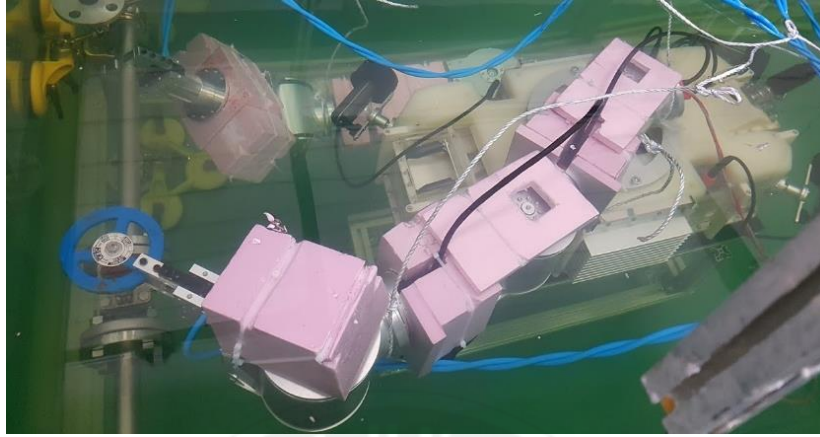


Fig. 6 Valve operation of UVMS

However, the weighting matrix of control was fixed regardless of the external environment. In this study, the UVMS designed for the TTURT was revised and used for the new AUV, AURORA. Using this, we introduce an algorithm for newly determining the weighting matrix of UVMS. We use this to introduce a new algorithm to determine the weighting matrix that can reduce torque than the previous study.

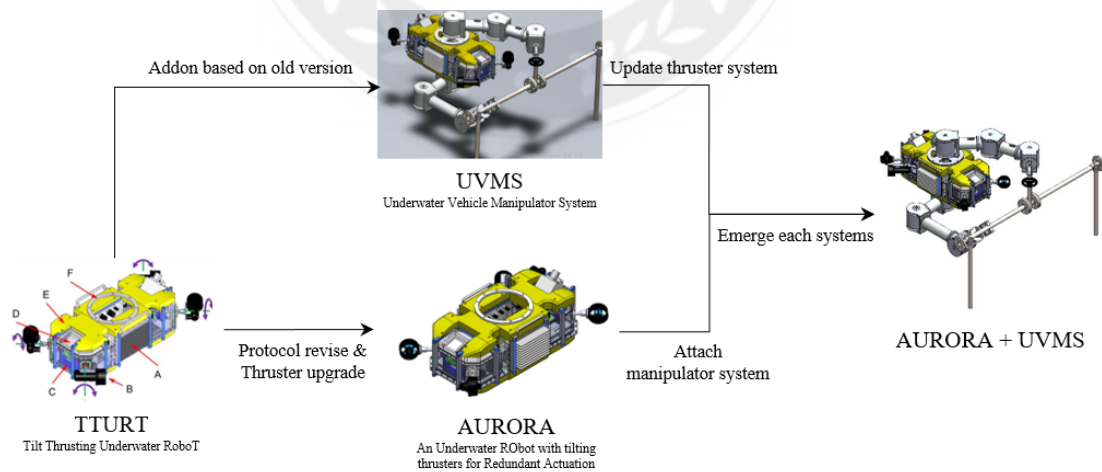


Fig. 7 History of underwater robot project

Table 1 Comparison of each underwater robot research project

	TTURT (2014)	UVMS (2019)	AURORA (2020)
Research topic	Hovering Control of an Underwater Robot with Tilting Thrusters Enabling Various Works	Cooperative operation of underwater robotic vehicle and dual-arm manipulator	Optimal hovering control of an underwater robot with redundant tilting thrusters
Thruster	Seabotix BTD 150 [2.2kgf] Two thrusters connected to one motor		Blue Robotics T200 [5.25 kgf] One thruster – one motor
Tilt angle	Connected one motor Discontinuous (0° - 90° - 180° - 270°)		Continuous
Protocol	RS232, CAN, etc		CAN

Section 3 Research purpose

In this study, we show a real-time torque distribution to reduce the torque of a parallel underwater manipulator. The purpose of this study is to reduce the overall burden of torque on the manipulator joint. In order to evaluate this, the maximum torque of each joint is minimized and the load torque of the joint is observed over time. Two experiments were conducted to compare the results to show a reduction in torque burden. First, we check the manipulator load torque during simple control through a randomly set fixed weighting matrix that was fixed in the previous study. After that, the next experiment is applying a new real-time torque distribution algorithm. By comparing the difference between these two cases, we show that the algorithm presented in this study can lower the torque.

Chapter 2 Foundation of AURORA and manipulators

Section 1 AUV – Manipulator overall structure

The robot is composed by attaching underwater manipulators to the top and bottom of AURORA. AURORA moves and shared the force for underwater work by using the four rotatable thrusters attached to the main body. This study is based on three studies, TTURT, AURORA, and UVMS, presented in Chapter 1. [11] [12] [13]

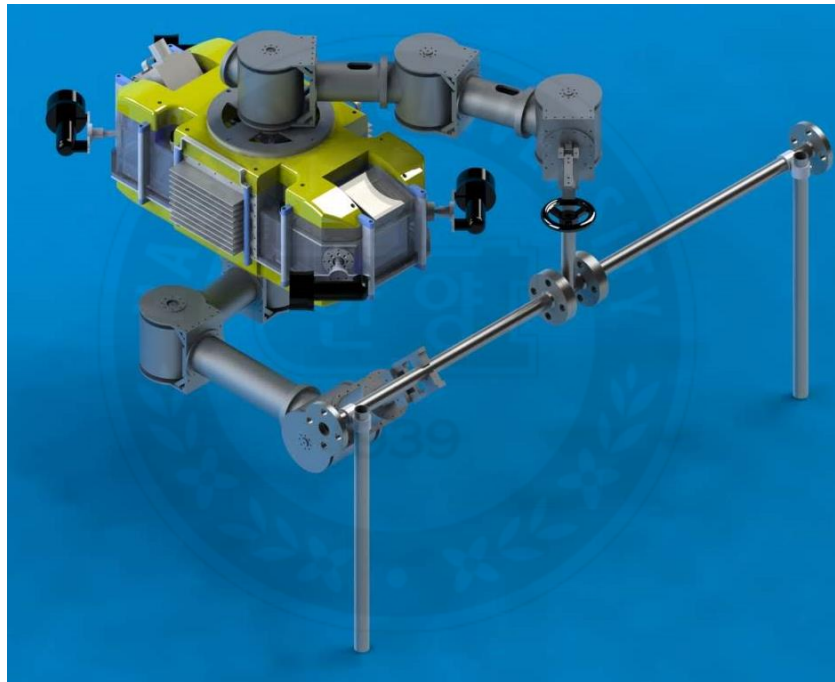


Fig. 8 The entire main body and manipulator used in this study

Section 2 AURORA body hardware structure

In AURORA, modules that share each function are combined by aluminum frames. And the connecting part of the work terminal is connected up and down of AURORA. There are 5 types of modules, each of which has a front head module, a rear tail module, a camera module, a 12V power module, and an 18V power

module.

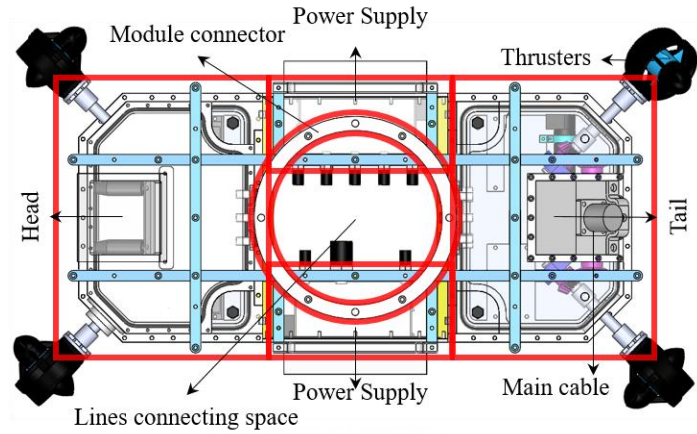


Fig. 9 AURORA Parts Structure

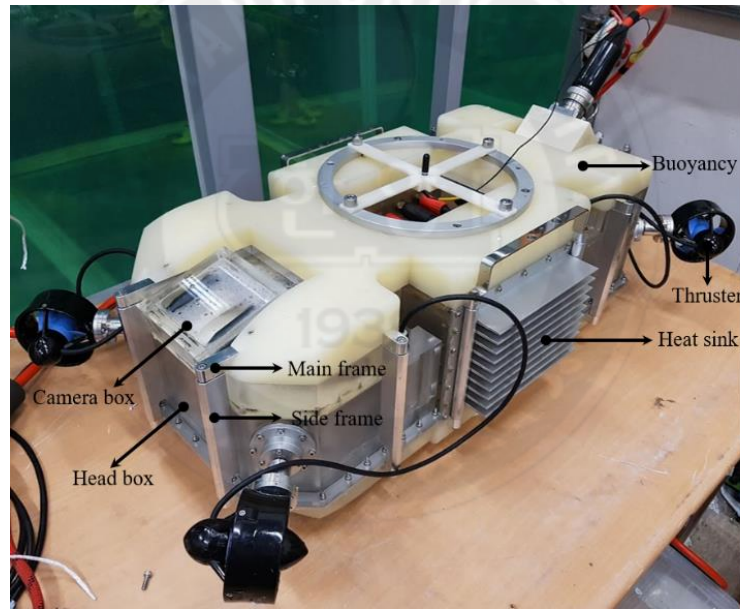


Fig. 10 AURORA appearance and structure

First, the head module and tail module are dedicated to drive the thruster. For alignment of the angle of the thruster, a photodiode used for motor, and a motor driver that controls the tilting angle and thrust force is also included. In addition, an IMU, a water pressure sensor is included to specify a position underwater. In the casing, the upper part of the acrylic material, which is 10 mm thick, and the aluminum base plate are combined with a number of screws with an O-ring to

make it waterproof.

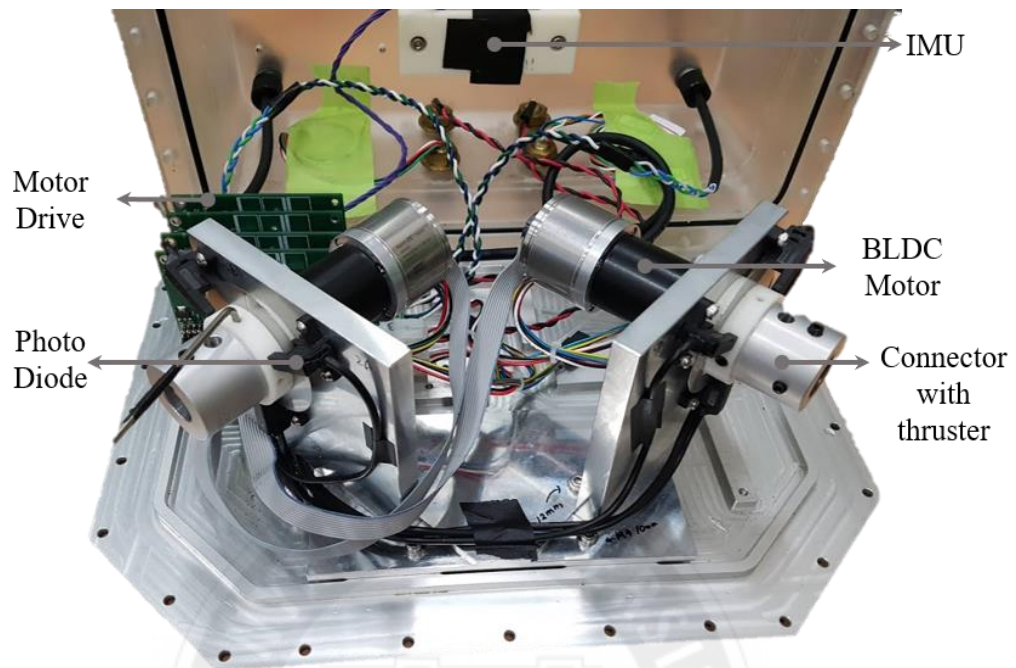


Fig. 11 AURORA drive-related parts

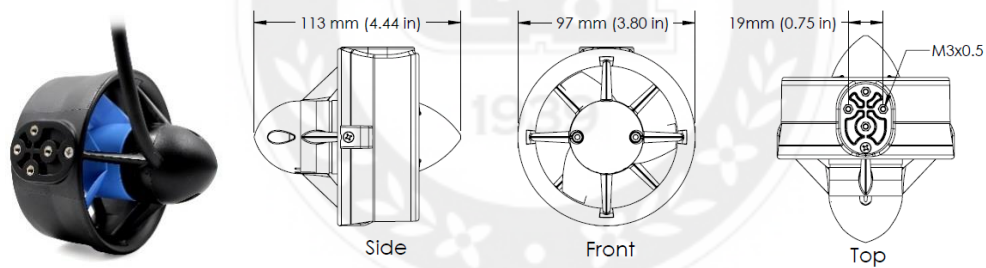


Fig. 12 Appearance and structure of thruster T200 used in aurora

Table 2 T200 Specification

Blue Robotics T200 thruster.	
Material	Polycarbonate plastic, 316 stainless steel.
Number of blades	3
Diameter	10cm
Operating volts	7-20V (32A)
Full throttle force	5.2kgf
Minimum Thrust	0.02kgf
Full throttle power	645W
Weight	344g
Underwater weight	156g

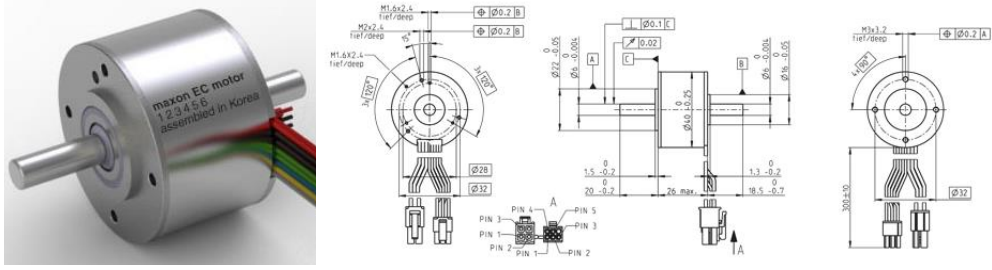


Fig. 13 Tilting motor EC-i 40

Table 3 EC-I 40 specification	
EC-i 40 Ø40 mm, brushless, 50 Watt	
Nominal voltage	12V
Nominal speed	9840RPM
Nominal torque	36.8mNm
Nominal current	4.1A
Stall torque	432mNm
Weight	170g

In the previous study, some modeling of the motors was performed, and the model was used as it was for controlling the robot.

Table 4 Thrust, tilting motor modeling [13]

Modeling of Thruster motor for compensating dead zone	Modeling of Thruster motor for delay time	Modeling of tilting motor for delay time
$F_{SS} = \begin{cases} 3.96 \times 10^{-6} \Omega^2 & \text{for } \Omega > 300 \\ 3.30 \times 10^{-6} \Omega^2 & \text{for } \Omega < -300 \\ \text{Dead zone} & \text{for } -300 \leq \Omega \leq 300 \end{cases}$ <p>F_{SS} : thrust force in steady state</p>	$\theta_{n+1} = \begin{cases} \theta_n & \text{for } \theta_n = \theta_d \\ \theta_n + 670t_s & \text{for } \theta_n < \theta_d \\ \theta_n - 670t_s & \text{for } \theta_n > \theta_d \end{cases}$	$\Omega_{n+1} = \begin{cases} \Omega_n & \text{for } \Omega_n = \Omega_d \\ \Omega_n + 670t_s & \text{for } \Omega_n < \Omega_d \\ \Omega_n - 670t_s & \text{for } \Omega_n > \Omega_d \end{cases}$

The camera box is located at the top of the head part, and the camera for underwater situations observation is located.

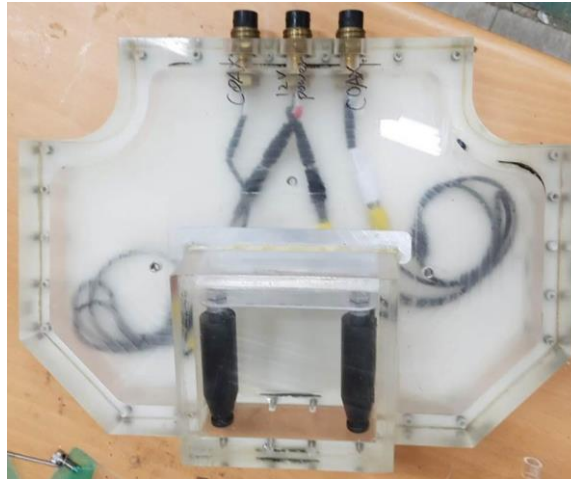


Fig. 14 Camera box

And the power modules that are responsible for the main power of AURORA are located on the left and right sides. It is in charge of power for all control boards of AURORA and power for thrusters. [13]

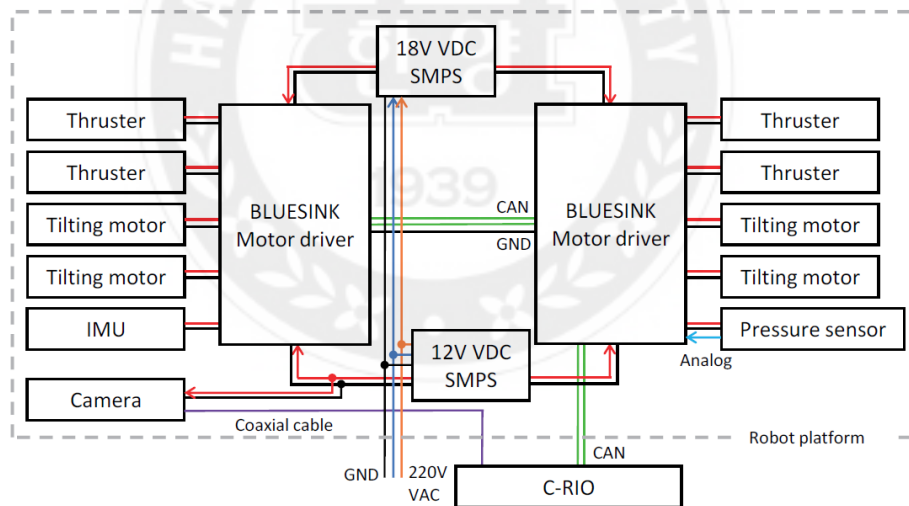


Fig. 15 Signal map of the robotic platform. [13]

Table 5 Electric components of AURORA

Components	EA	Specification
Thruster	4	Blue Robotics T200
Tilting motors	4	Maxon
Thrust drivers	2	Bluesink
Controller	1	NI CRIO 9082
Inertia Measuring Unit	1	EBIMU-9DOFFV4 E2BOX
Camera	2	Vision Hitech VH211HQ
Pressure transducer	1	Sensotec FP2000
DC power supply	2	TDK Lambda HWS600
Waterproof connector and cable		SubConn Mycro series etc.
Tether		MacArtney 6120B TV Cable

Section 2 Underwater manipulator hardware structure

The underwater manipulator consists of a joint where a motor is located to generate torque, and a pipe-shaped connection part that connects between the joints. The connection part is exposed to water, and the joint part is designed to be waterproof to block water. [11]

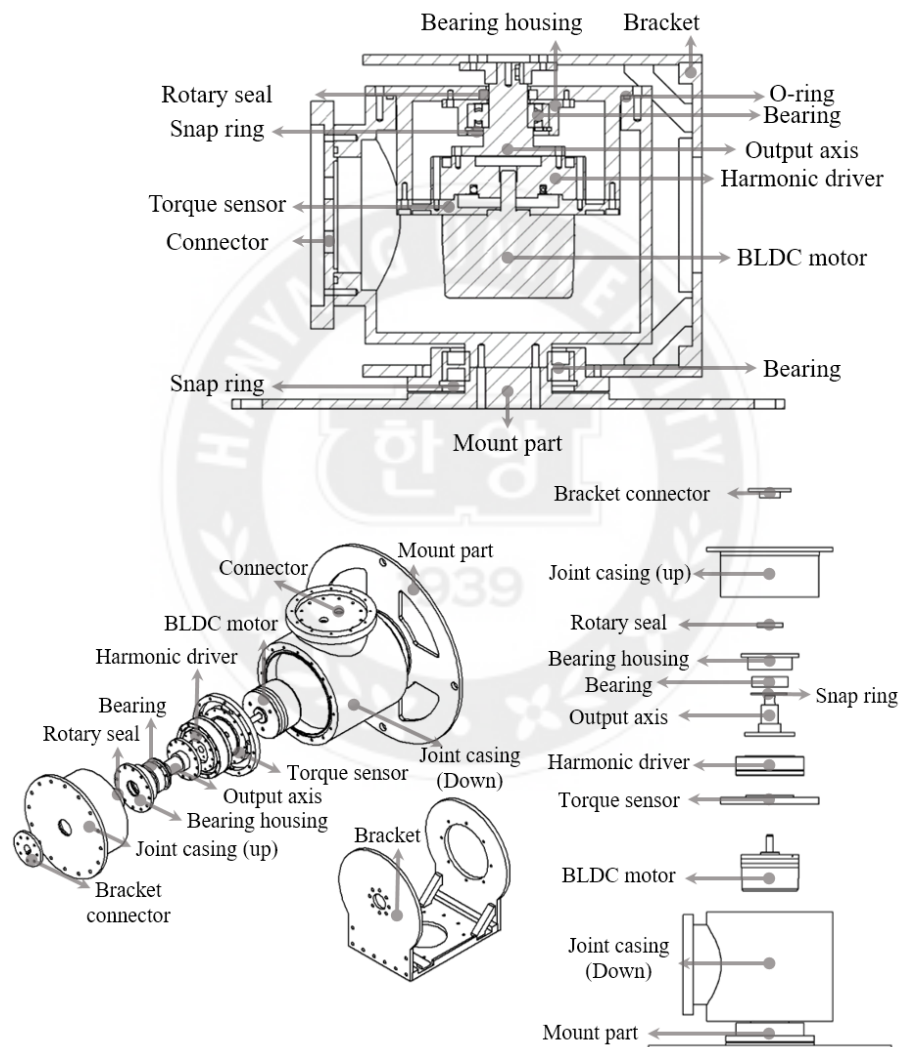


Fig. 16 Structure and exploded view of the manipulator joint

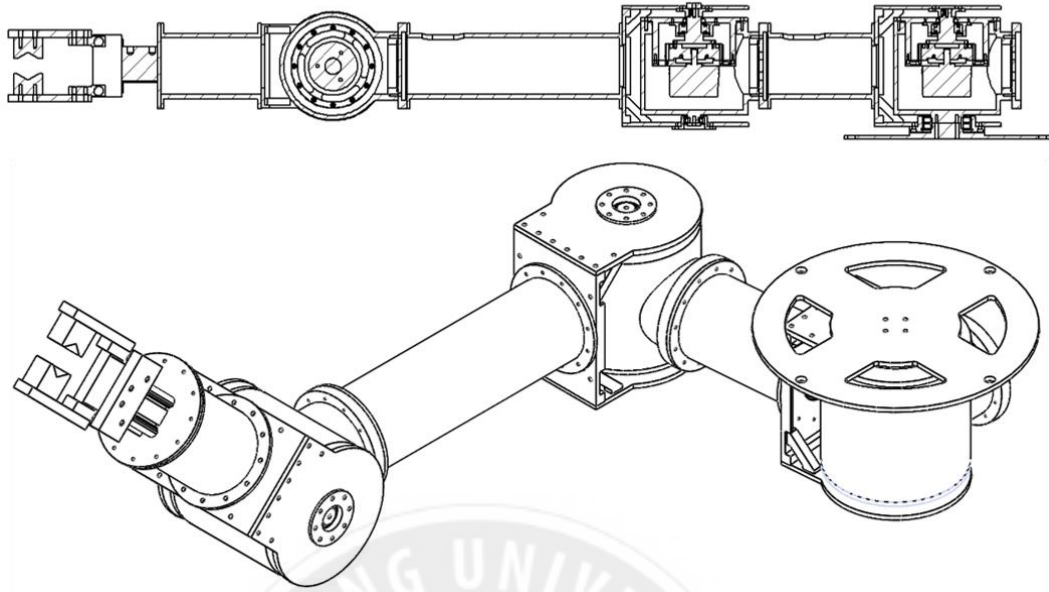


Fig. 17 Assembled Clamping Manipulator

In the case of the joint, the basic material is aluminum 6061. The casing is separated into a top cap and a bottom portion, and is waterproofed with an O-ring and 12 bolts.



Fig. 18 Manipulator joint casing

The upper casing part is coupled with an encoder sensor, a torque sensor, and a drive unit assembled with a motor. The penetrating drive shaft is connected to the external bracket to control the manipulator. A rotary seal enters to waterproof

the hole between the drive shaft and the upper casing. In addition, due to friction of the rotary seal, torque is generated due to friction even when there is no load. Therefore, a compensation process using a friction model is required to correct this torque in the sensor.

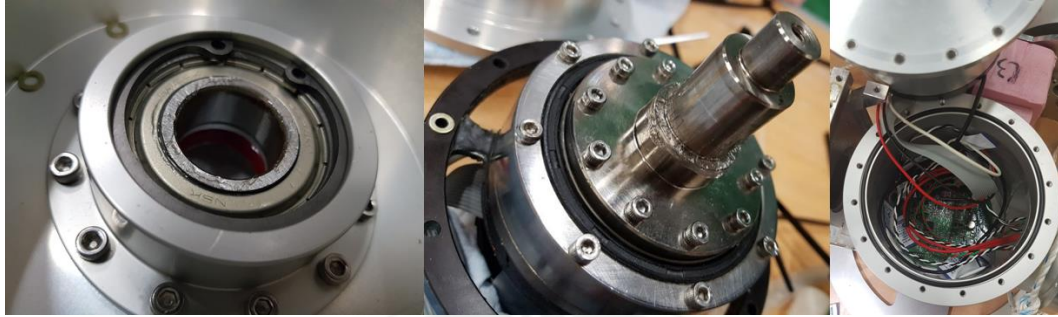


Fig. 19 Rotary seals that block leakage in the direction of the drive shaft, the motor driver and wires inside the drive shaft and casing

The bracket and drive shaft are connected, and the bracket is also connected to the bearing on the opposite side of the casing. Nevertheless, in addition to the torque in the axial rotation, an error is generated in the torque sensor in the horizontal twist. To prevent this twist, a buoyant material was produced and attached to the manipulator. The buoyant material was manufactured by processing XPS (Extruded Polystyrene Insulation Board) which is inexpensive and has low density. Based on the Archimedes principle, the buoyancy equation was calculated for the volume of the buoyant material that maintains the neutral buoyancy. [14]

$$m_{AURORA}g + \rho_{Buoyancy}V_{Buoyancy}g - \rho_{water}V_{Buoyancy}g = 0 \quad (1)$$

$$V_{Buoyancy} = \frac{m_{AURORA}}{\rho_{water} - \rho_{Buoyancy}} \quad (2)$$

Table 6 Electric components of the dual-arm manipulator. [11]

Components	EA	Specification
Motor	6	Maxon EC 60 flat, 24V 100W
Reducer	6	SBB SCSD-17-100-2UF
Motor driver	6	Robotro customized
Controller	1	NI CRIO 9082
Torque sensor	6	SETECH customized
DC power supply	1	24V 1500W
Waterproof cable		Subconn Micro series



Fig. 20 Attached buoyancy material

Table 7 Buoyancy calculation result by manipulator part

	EndEffector	EndEffector WithPipe	JointModule	JointModule Mounted	PipeLong	PipeShort
Weight [kgf]	1.3	3.05	5.8	7	1.5	0.8
Volume [m ³]	0.0003	0.0005	0.002	0.003	0.0005	0.0002
Buoyancy [kgf]	0.329	0.5694	2.876	3.215	0.508	0.271
Underwater weight [kgf]	0.970	2.480	2.923	3.784	0.991	0.528
Buoyancy volume [m ³]	0.001	0.002	0.003	0.003	0.001	0.0005

Section 2 Underwater manipulator friction compensation

Torque due to friction is generated in the underwater manipulator even when the load is not applied due to the friction of the rotary seal and the weight and resistance of the bracket. In order to remove this torque, friction modeling of the rotary seal and bracket was performed using a Dahl model. [15] [16]

$$\frac{dF}{dx} = \sigma \left(1 - \frac{F}{F_c} \operatorname{sgn} v\right)^\alpha, \quad \frac{dF}{dt} = \sigma \left(1 - \frac{F}{F_c} \operatorname{sgn} v\right)^\alpha v, \quad (3)$$

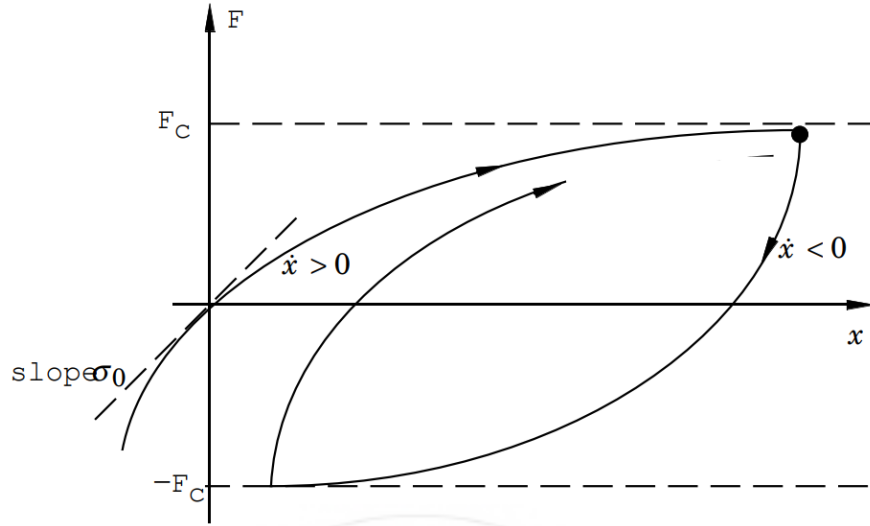


Fig. 21 Dahl model friction graph [15]

When friction is compensated with the Dahl model, large friction can be corrected. However, it is difficult to correct the friction when the torque is greatly changed, and as a result, a value remains in the form of noise. So, after this, additional correction is performed using Kalman filter and PID.

Section 3 Underwater manipulator analysis and control

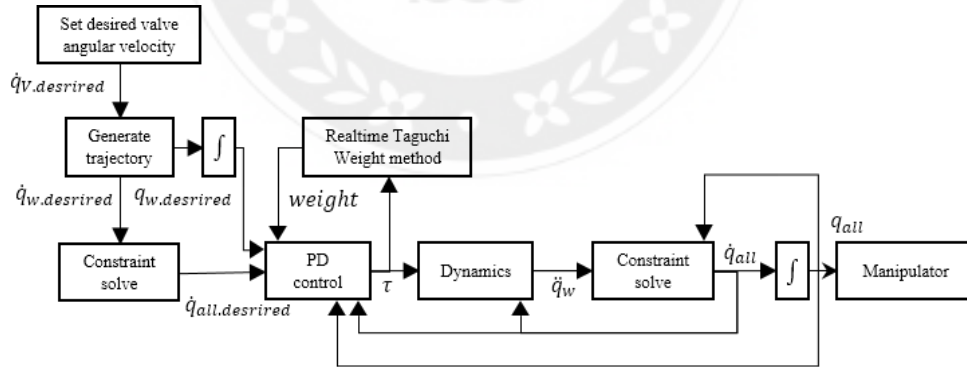


Fig. 22 Manipulator Control Flowchart

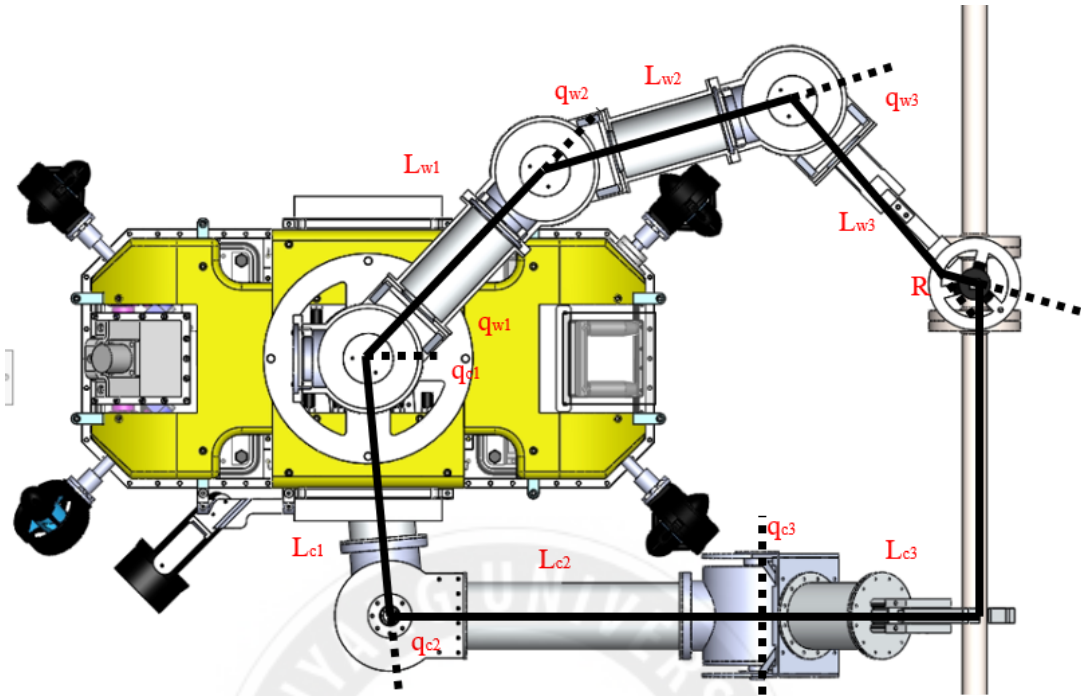


Fig. 23 AURORA – Manipulator Diagram

The control process of the manipulator consists of manipulator trajectory generation, PD control, dynamics analysis, and driving angle and total angle conversion using the constrained Jacobian. As a first step, set $\dot{q}_{v.desired}$ at what speed the valve will move. In this study, the valve work is done at an angle of 45 degrees. The valve motion was set to the valve rotation at an angular velocity of $2/32 \pi$ in the counterclockwise direction.

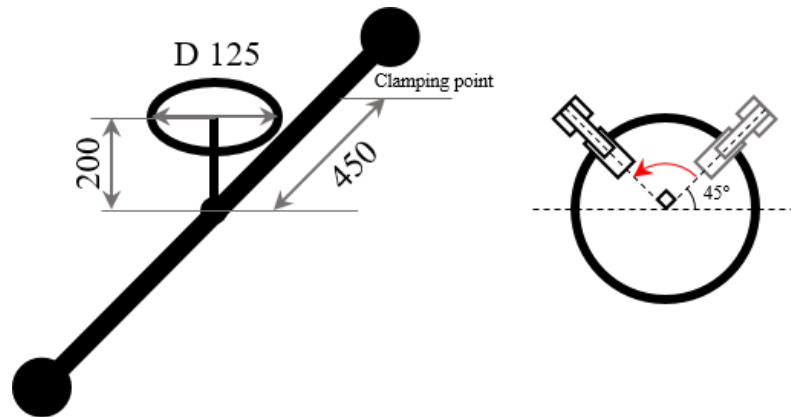


Fig. 24 Valve dimensions and rotation angle

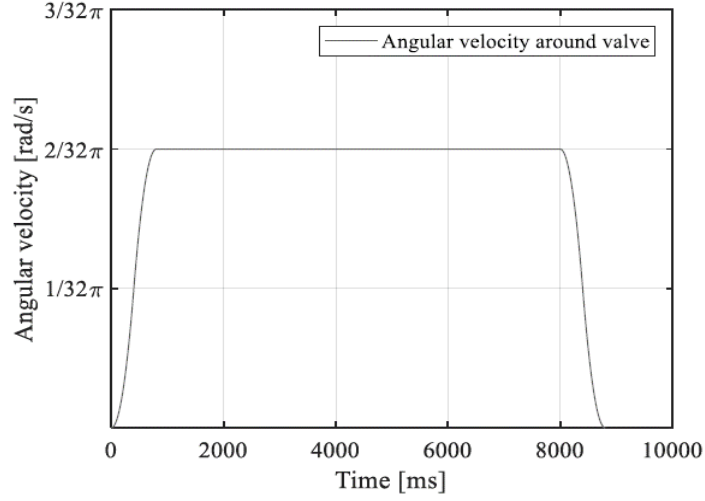


Fig. 25 Valve rotation speed over time [13]

In order to find the optimal path to rotate the valve, the optimal criterion was to minimize the norm term of the speed of the actuated joint.

$$\min(\|\dot{\mathbf{q}}_r\|) \quad (4)$$

Considering the definition of Constraint Jacobian, the square of the norm term changes to the follow:

$$\dot{\mathbf{q}}_r = \mathbf{\Gamma} \dot{\mathbf{q}}_w \quad (5)$$

$$\|\dot{\mathbf{q}}_r\|^2 = \dot{\mathbf{q}}_w^T \mathbf{\Gamma}^T \mathbf{\Gamma} \dot{\mathbf{q}}_w \quad (6)$$

In addition, the following equation is established by the basic definition of Jacobian.

$$\dot{\mathbf{q}}_v = (\mathbf{J}_w + \mathbf{J}_v \mathbf{\Phi}) \dot{\mathbf{q}}_w = \mathbf{J}_f \dot{\mathbf{q}}_w \quad (7)$$

$$\dot{\mathbf{q}}_{w.desired} = \mathbf{J}_f^\dagger \dot{\mathbf{q}}_{v.desired} \quad (8)$$

$$\mathbf{J}_f^\dagger = (\mathbf{\Gamma}^T \mathbf{\Gamma})^{-1} (\mathbf{J}_f (\mathbf{\Gamma}^T \mathbf{\Gamma})^{-1})^\dagger \quad (9)$$

That is, when $\dot{\mathbf{q}}_{v.desired}$ is determined, $\dot{\mathbf{q}}_{w.desired}$ is also determined. Once $\dot{\mathbf{q}}_{w.desired}$ has been determined, the restrained Jacobian can be used to find all angular velocity $\dot{\mathbf{q}}_{all}$. [17]

$$\dot{\mathbf{q}}_{all} = \mathbf{\Lambda} \dot{\mathbf{q}}_w \quad (10)$$

PID control is possible because $\dot{\mathbf{e}} = \dot{\mathbf{q}}_{w.d} - \dot{\mathbf{q}}_w$ can be calculated when $\dot{\mathbf{q}}_{all}$ is

derived and $\mathbf{e} = \mathbf{q}_{w,d} - \mathbf{q}_w$ can be calculated by integrating per unit time. It is possible to calculate a value to be a target value using PD control.

$$\begin{aligned}\boldsymbol{\tau}_{r.desired} &= (\boldsymbol{\Gamma}^T)^\# (\mathbf{K}_v \dot{\mathbf{e}} + \mathbf{K}_p \mathbf{e}) + \boldsymbol{\tau}_{comp} \\ &= (\boldsymbol{\Gamma}^T)^\# (\mathbf{K}_v \dot{\mathbf{e}} + \mathbf{K}_p \mathbf{e}) + (\boldsymbol{\Gamma}^T)^* \mathbf{J}_b^T (-\mathbf{f}_d) \\ (\boldsymbol{\Gamma}^T)^\# &= \mathbf{W}^{-1} (\boldsymbol{\Gamma}^T \mathbf{W}^{-1})^\dagger, (\boldsymbol{\Gamma}^T)^* = \mathbf{W}_d^{-1} (\boldsymbol{\Gamma}^T \mathbf{W}_d^{-1})^\dagger\end{aligned}\quad (11)$$

If $\boldsymbol{\tau}_{r.desired}$ is derived, it is possible to calculate the angular acceleration $\ddot{\mathbf{q}}_w$ of the driving joint that inverses the manipulator dynamics equation to generate a torque corresponding to $\boldsymbol{\tau}_{r.desired}$.

The dynamic equation of a typical underwater robot body is derived as follows. [18] Detailed calculation results are presented in previous studies. [12]

$$\mathbf{M}_v \dot{\mathbf{v}} + \mathbf{C}_v(\mathbf{v})\mathbf{v} + \mathbf{D}_v(\mathbf{v})\mathbf{v} + \mathbf{g}_v = \boldsymbol{\tau}_v \quad (12)$$

And, based on a fixed ground coordinate system, the dynamic equation of the manipulator is derived as follows.

$$\mathbf{M}_m \ddot{\mathbf{q}} + \mathbf{C}_m(\mathbf{q})\dot{\mathbf{q}} + \mathbf{D}_m(\mathbf{q})\dot{\mathbf{q}} + \mathbf{g}_m = \boldsymbol{\tau}_m \quad (13)$$

Because the AUV and the manipulator work together, we have to think of the mutual effects. If you combine the two into the Newton–Euler method, you will get the following.

$$\begin{aligned}\mathbf{M}(\boldsymbol{\zeta})\dot{\boldsymbol{\zeta}} + \mathbf{D}(\mathbf{q}, \dot{\mathbf{q}}, \boldsymbol{\zeta})\boldsymbol{\zeta} &= \boldsymbol{\tau} \\ \mathbf{M}(\boldsymbol{\zeta}) &= \begin{bmatrix} \mathbf{M}_v + \mathbf{H}_w(\mathbf{q}_w) + \mathbf{H}_c(\mathbf{q}_c) & \mathbf{M}_{cw}(\mathbf{q}_w) & \mathbf{M}_{cc}(\mathbf{q}_c) \\ \mathbf{M}_{cw}^T(\mathbf{q}_w) & \mathbf{M}_w(\mathbf{q}_w) & \mathbf{0} \\ \mathbf{M}_{cc}^T(\mathbf{q}_c) & \mathbf{0} & \mathbf{M}_c(\mathbf{q}_c) \end{bmatrix}, \\ \mathbf{D}(\mathbf{q}, \boldsymbol{\zeta}) &= \begin{bmatrix} \mathbf{D}_v(\mathbf{v}) + \mathbf{D}_{w1} + \mathbf{D}_{c1} & \mathbf{D}_{w2} & \mathbf{D}_{c2} \\ \mathbf{D}_{w3} & \mathbf{D}_w & \mathbf{0} \\ \mathbf{D}_{c3} & \mathbf{0} & \mathbf{D}_c \end{bmatrix}, \boldsymbol{\zeta} = [\mathbf{v}^T, \mathbf{q}_w^T, \mathbf{q}_c^T]^T\end{aligned}\quad (14)$$

The calculation results for this were introduced in previous studies. [17]. The dynamic equation of UVMS fixed to the body can be summarized as follows [19].

$$\hat{\mathbf{M}}\ddot{\mathbf{q}}_u + \hat{\mathbf{D}}\dot{\mathbf{q}}_u = \boldsymbol{\Gamma}^T \boldsymbol{\tau}_r \quad (15)$$

$$(\hat{\mathbf{M}} = \mathbf{\Lambda}^T \mathbf{M} \mathbf{\Lambda}, \hat{\mathbf{D}} = \mathbf{\Lambda}^T \mathbf{M} \dot{\mathbf{\Lambda}} + \mathbf{\Lambda}^T \mathbf{D} \mathbf{\Lambda})$$

If we transform these equations to calculate $\ddot{\mathbf{q}}_u$:

$$\ddot{\mathbf{q}}_u = \hat{\mathbf{M}}^{-1} (\mathbf{\Gamma}^T \boldsymbol{\tau}_r - \hat{\mathbf{D}} \dot{\mathbf{q}}_u) \quad (16)$$

That is, it is possible to calculate how much angular acceleration the drive motor should move to achieve the target torque using this equation. This recalculates the constrained Jacobian to recalculate the angular behavior of the entire joint from the driving joint. Integrating the $\dot{\mathbf{q}}_{all}$ thus produced as a unit time allows the angle of all joints to be obtained, and the manipulator is controlled using the angle value.



Chapter 3 Real-time torque distribution algorithm

Section 1 Taguchi method

Showing the results of the experiment effectively and reducing the number of experiments is major concern. The concern was established to the design of experiment (DOE). DOE is a statistical approach to designing an experiment, to reduce costs and increase the effectiveness of experiments through clearer evaluation indicators. Among these DOE, Taguchi method is meaningful in that it is a comprehensive methodology that not only reduces the number of experiments, but also quantifies performance evaluation to evaluate efficiency and improve production quality. As it is a process of finding the optimal value while reducing the number of experiments, it may overlap somewhat with the optimization. However, optimization technique like SQP (Sequential quadratic programming), it can be said to be a wider range of areas that include this optimization technique. And it has the advantage of being able to conduct experiments more efficiently based on the experience of the experiment designer. In addition, unlike the general optimization method that repeats until the target value is reached, the number of experiments can be predicted through an orthogonal matrix.

The Taguchi method was proposed by Dr. Kenichi Taguchi. It is also called a robust design because it has a purpose to ensure the performance of the product in various user condition. The Taguchi method began in 1950 under the supervision of Dr. Taguchi at the Japanese Inax company and has been applied as a practical methodology in the industry. [20] This was organized as a booklet by the Union of Japanese Scientists and Engineers (JUSE) in 1959, and later began to be studied academically since the 1980s. [21] As the start was practically started in the actual industrial site, it has a disadvantage in that it is relatively weak on the theoretical basis. However, it is regarded as an effective quality management methodology because it has been recognized for its advantages

through success cases and research in additional industries.

Table 8 Taguchi method procedure [20]

Step	Tasks
Problem formulation	Define problem Selection of characteristic values Confirmation of measurement method Design variable selection and level determination Determination of application method, level determination
Design of experiment (DOE)	Orthogonal table composition Data collection
Data analysis	SN ratio calculation Determining significant effects Determination of optimal conditions
Confirmation	Confirmation experiment, Verification

The process of the Taguchi method is to repeat the steps of problem formulation, experiment planning, experimentation, results analysis, and future experiment planning. Problem formulation is a step to describe limitation and what variables are being experimented. Since it is the step of specifying the design variables and conditions to be found, it has an important meaning as the first step in determining the direction of the entire experiment. The factors that can be changed by the experiment planner during the experiment are called “design variables” . The result value that is intended to approach the maximum, minimum, or specific value through this is called the “objective function” . Through experiments, various design variables and objective function values are changed. The process of changing design variables can be repeated to maximize performance. In addition, it can be summarized that the number of repetitions is reduced by methods such as orthogonal array (OA), so that good results can be obtained while reducing cost and time. As a starting point, planner need to think deeply and in detail what variables are the design variables that can affect the target variable you are looking for. This is also an important field of study, which was established as a research field called factor analysis. In addition, several charts under the name of factor analysis chart were developed as tools to help with factor analysis.

The experiment planning is the stage of planning the details of the experiment to determine the basis for proving the theory by performing several experiments depending on which variables are used for experiments. First, we need to reduce the number of experiments and find a suitable value for the target variable. The level of design experiments is set by changing the design variables set during problem formulation. Also, when variables are changed according to the level, it is determined whether they are correlated or independent of each other. We organize these relationships and calculate the degree of freedom (DOF) of the design variables based on this relationship. And based on this, OA is determined and OA is constructed by considering the correlation between each element using a linear graph. This OA utilizes the verticality of the vector to greatly reduce the number of experiments that increase in the squared level of the variable. This is a role that allows you to proceed with only the essential experiments, except for all experiments that are difficult to show a significant effective relationship. This OA is determined to have a higher degree of freedom than the sum of the degrees of freedom of the design variables. The greater the degree of freedom and the greater the number of experiments determined through OA. So, it is selected as the smallest OA that can be selected while being larger than the sum of design variables.

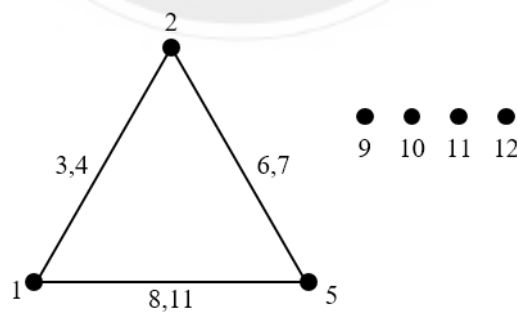


Fig. 26 Linear graph used for OA construction

After the experiment plan, the experiment is conducted in the designated user condition based on the OA that was configured during the experiment plan.

After the experiment, the results from the experiment are arranged, and the experiment is planned again. First, S/N Ratio (Signal-to-Noise Ratio) is used to evaluate the performance under each design variable and user condition. The S/N Ratio was originally used for electronic communication to refer to the ratio of noise that interferes with signal and signal interpretation. It is used by Dr. Taguchi as a representative value of performance in the Taguchi method. How to convert the S/N Ratio depends on whether the objective function should be small, large, or a specific value. The S/N Ratio is an indicator of performance regardless of characteristics. Therefore, the larger the S/N Ratio means the better performance. That is, it can be said that the level of the design variable in which the S/N Ratio is large has better performance. Then, the search range is reset to the level of the design variable with a large SN ratio, and the previous process is repeated with a better value.

Table 9 S/N Ratio according to the objective function value [21]

Smaller-the-better (STB),	$SN_{STB} = -10 \log_{10} \left(\frac{1}{n} \sum_{i=1}^n y_i^2 \right)$
Nominal-the-best (NTB),	$SN_{NTB} = -10 \log_{10} \left(\frac{1}{n-1} \left(\sum_{i=1}^n (e_i^2) - S \right) \right), \quad S = \frac{1}{n} \left(\sum_{i=1}^n (e_i) \right)^2$
Larger-the-better (LTB)	$SN_{LTB} = -10 \log_{10} \left(\frac{1}{n} \sum_{i=1}^n \frac{1}{y_i} \right)$

Section 2 Real-time Torque Squared Sum Minimization Algorithm

As stated in the introduction, there can be a variety of error factors that can't be predicted underwater. In order to control the manipulator in this changing external environment, the manipulator algorithm of this study calculates the weighting matrix based on sensor values in real time. This reduces the risk of manipulator breakage and control failure due to strong internal forces caused by external changes.

The weighting matrix is meaningful because the operator can more intuitively

adjust the weight of each driving component. The condition of the manipulator such as damage to each driving component and abnormality of the sensor can be changed when the manipulator is operated for a long time. Considering this, it is meaningful to intuitively control by adjusting the elements of the weighting matrix to reduce the load of the mechanical component. However, it is difficult to be sure that the weighting matrix determined according to the operator's judgment is an appropriate decision for the environment. Therefore, in addition to the operator's decision, it is also necessary to assist with the weighted matrix decision by reflecting the part that is difficult for humans to detect.

The goal of the algorithm is to reduce the burden of torques every hour by distributing the load to the thruster or other joints. It is possible to reduce the torque required by the drive motor of each joint and also has the advantage of improving the life of manipulator joints by reducing the burden on the joint. In addition, the sum of squares of torques is used as a target function. Since it starts from the concept of dispersion of torque distribution, there is an advantage that the torque is reduced as a whole.

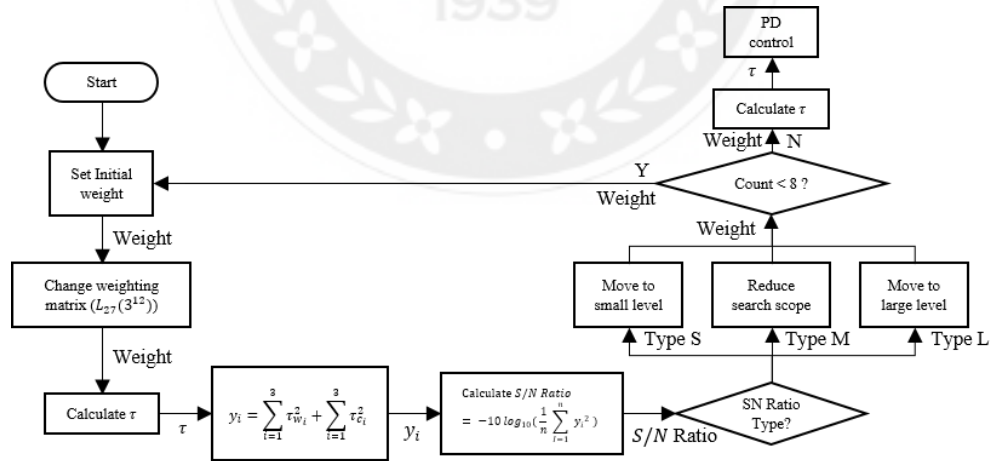


Fig. 27 Real-time Taguchi Torque Squared Minimization Algorithm Flowchart

The real-time optimization method presented in this paper aims to determine the weighting matrix in real time using the Taguchi method using sensor values. Just as the Taguchi method experiments and evaluates to find the optimal value

of a design variable, in this algorithm, it computes the experiment corresponding to the experiment and evaluates the weight change to repeat. First, we begin the formalization of the problem. The design variables to be found are positive elements $w_1 \sim w_{12}$ entering the weighting matrix, and the objective function for evaluating the performance is the sum of squares of torques of each joint.

$$\begin{aligned} \text{Given } Weight &= [w_1, w_2, w_3, w_4, w_5, w_6, w_7, w_8, w_9, w_{10}, w_{11}, w_{12}] \\ \text{minimize } &(\tau_{w_1}^2 + \tau_{w_2}^2 + \tau_{w_3}^2 + \tau_{c_1}^2 + \tau_{c_2}^2 + \tau_{c_3}^2) \\ \text{subject to } &Weight > 0 \end{aligned}$$

Fig. 28 Problem formulation of a real-time torque sum-of-squares minimization algorithm

The design variables for minimizing the sum of squared torques are the 12 elements that make up the weighting matrix. Changing one element does not change the other. That is, they are design variables that are independent of each other and have no correlation. In order to determine whether to increase or decrease the values in the next operation, these design variables will be divided into three levels: the original value, the increment value, and the decrease value. That is, each of the twelve elements has three stages, and $L_{27}(3^{12})$ is represented by the corresponding OA. [21][22] The degrees of freedom are $(3-1) * 12 = 24$. Looking at the degrees of freedom among the vertical matrices presented, $L_{18}(2^1 \times 3^7)$ has 15 degrees of freedom and $L_{27}(3^{13})$ has 26 degrees of freedom. The vertical matrix is determined by $L_{27}(3^{13})$. For reducing the amount of computation, a vertical matrix corresponding to $L_{27}(3^{12})$ is generated and used using PIAAnO Sampler.

Table 10 Orthogonal array for weight calculation

N	1	2	3	4	5	6	7	8	9	10	11	12
1	1	1	1	1	1	1	1	1	1	1	1	1
2	1	1	1	2	2	2	3	3	3	1	2	3
3	1	1	1	3	3	3	2	2	2	1	3	2
4	1	2	3	1	2	3	1	2	3	2	1	3
5	1	2	3	2	3	1	3	1	2	2	2	2
6	1	2	3	3	1	2	2	3	1	2	3	1
7	1	3	2	1	3	2	1	3	2	3	1	2
8	1	3	2	2	1	3	3	2	1	3	2	1
9	1	3	2	3	2	1	2	1	3	3	3	3
10	2	1	3	1	3	2	3	2	1	3	3	3
11	2	1	3	2	1	3	2	1	3	3	1	2
12	2	1	3	3	2	1	1	3	2	3	2	1
13	2	2	2	1	1	1	3	3	3	1	3	2
14	2	2	2	2	2	2	2	2	2	1	1	1
15	2	2	2	3	3	3	1	1	1	1	2	3
16	2	3	1	1	2	3	3	1	2	2	3	1
17	2	3	1	2	3	1	2	3	1	2	1	3
18	2	3	1	3	1	2	1	2	3	2	2	2
19	3	1	2	1	2	3	2	3	1	2	2	2
20	3	1	2	2	3	1	1	2	3	2	3	1
21	3	1	2	3	1	2	3	1	2	2	1	3
22	3	2	1	1	3	2	2	1	3	3	2	1
23	3	2	1	2	1	3	1	3	2	3	3	3
24	3	2	1	3	2	1	3	2	1	3	1	2
25	3	3	3	1	1	1	2	2	2	1	2	3
26	3	3	3	2	2	2	1	1	1	1	3	2
27	3	3	3	3	3	3	3	3	3	1	1	1

The torque is calculated by the weighting matrix in which the weighting matrix is corrected by adding or subtracting from the starting weighting matrix value by the increment/decrement value. Of these calculated 6 torques, the absolute value with the largest absolute value is selected as y_i . S/N Ratio is calculated using these results. Since the goal is to minimize the maximum absolute torque, this S/N Ratio is calculated in case for smaller-the-better.

$$SN \text{ Ratio} = -10 \log_{10} \left(\frac{1}{n} \sum_{i=1}^n y_i^2 \right) \quad (17)$$

The S/N Ratio calculated becomes a 12*3 matrix, which corresponds to three levels of change of elements in each weighted matrix. The calculated S/N Ratio becomes a 12*3 matrix, 12 rows of design variables, and columns corresponding

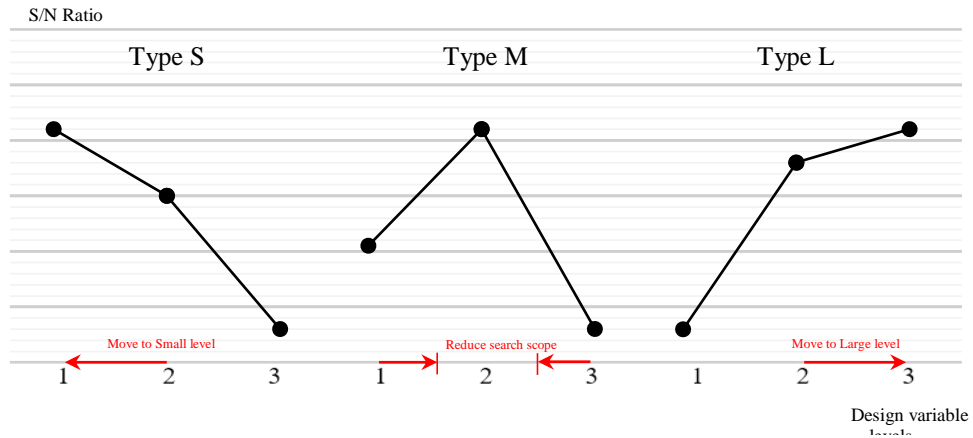


Fig. 29 Type of S/N Ratio and design variable aspects after that

to level 3 stages. The larger the S/N Ratio means the better the performance. In order to reduce the absolute value of the maximum torque, the S/N Ratio should be set to a large value. At this time, depending on the value of the S/N Ratio, determine how to modify the weighting matrix value when repeating this next operation. According to the position of the maximum value of the S/N Ratio value, the target function is determined to be the larger value among the three design variables in the next step. For example, when the maximum value of the S/N Ratio is at level 1, the value that becomes the starting point in the next operation is changed to a weighted matrix element value corresponding to each level 1. If the maximum value is at level 2, it means that the maximum value exists between levels 1 to 3, so it is necessary to narrow the search range of optimal values through calculation. Therefore, the increase/decrease value is reduced by multiplying the increase/decrease value used when setting the level by a specific ratio to narrow the search range in the next operation. The experiment process up to this point is repeated from the next calculation. Through this, the maximum torque value can be made smaller, and the more iterations, the more weighted matrix the minimum torque value can be obtained.

Table 11 Set initial value and initial stage of weighting matrix

Design Variable		Level 1 [Decrease]	Level 2 [Initial]	Level 3 [Increase]
w_1	AURORA F_x	91	141	191
w_2	AURORA F_y	91	141	191
w_3	AURORA F_z	50	100	150
w_4	AURORA τ_ϕ	564	614	664
w_5	AURORA τ_θ	515	265	315
w_6	AURORA τ_φ	137	187	237
w_7	Working manipulator Joint W1	1090	1140	1190
w_8	Working manipulator Joint W2	1090	1140	1190
w_9	Working manipulator Joint W3	1090	1140	1190
w_{10}	Clamping manipulator Joint C1	1090	1140	1190
w_{11}	Clamping manipulator Joint C2	1090	1140	1190
w_{12}	Clamping manipulator Joint C3	1090	1140	1190

Algorithm Realtime Taguchi weight algorithm	
1	constantWeight = 100;
2	WeightLevelInitialValue = 50;
3	n_count = 8;
4	OptimalSearchScale = 50;
5	
6	while WeightCount < n_count
7	for N_exp = 1 : 1 : 27
8	for Taunum = 1 : 1 : 12
9	WeightOACal (Taunum,Taunum) = Weight(Taunum,Taunum) * ((100 +
10	OA(N_exp,Taunum)*WeightLevelValue(Taunum))/100);
11	end
12	PinvGammaT = inv(WeightOACal)*pinv(Gamma.' * inv(WeightOACal));
13	PinvGammaT_d = inv(Weight_d)*pinv(Gamma.' * inv(Weight_d));
14	tau = PinvGammaT * (Kp * Er + Kv * Er_dot) + PinvGammaT_d * (Gamma(1:6,:)).' * (-f_d);
15	y_OA(N_exp) = (tau(7)^2)+(tau(8)^2)+(tau(9)^2)+(tau(10)^2)+(tau(11)^2)+(tau(12)^2);
16	end
17	for NumAtoC = 1 : 1 : 3
18	MSD = zeros(12);
19	for NumSNRatioOrder = 1 : 1 : 9
20	for Num12 = 1 : 1 : 12
21	MSD(Num12) = MSD(Num12) +
22	(y_OA(W_selectionOrderMatrix(NumAtoC,NumSNRatioOrder,Num12)))^2;
23	end
24	end
25	for i = 1 : 1 : 12
26	SNRatio(i,NumAtoC) = -10*log10((MSD(i))/9);
27	end
28	end
29	for NumWElement = 1 : 1 : 12
30	[maxSNRatio, maxSNRatioIndex] = max(SNRatio(NumWElement,:));
31	if maxSNRatioIndex == 1 %S type (go Smaller)
32	Weight (NumWElement,NumWElement) = Weight (NumWElement,NumWElement) * ((100 -
33	WeightLevelValue(NumWElement))/100);
34	elseif maxSNRatioIndex == 2 %M type (go Center)
35	WeightLevelValue(NumWElement) = WeightLevelValue(NumWElement) *
36	(OptimalSearchScale/100);
37	elseif maxSNRatioIndex == 3 %L type (go Larger)
38	Weight (NumWElement,NumWElement) = Weight (NumWElement,NumWElement) * ((100
39	+ WeightLevelValue(NumWElement))/100);
40	end
41	end
42	WeightCount = WeightCount + 1;
43	end
44	PinvGammaT = inv(Weight)*pinv(Gamma.' * inv(Weight));
45	PinvGammaT_d = inv(Weight_d)*pinv(Gamma.' * inv(Weight_d));
	tau = PinvGammaT * (Kp * Er + Kv * Er_dot) + PinvGammaT_d * (Gamma(1:6,:)).' * (-f_d);

Chapter 4 Experiment and results analysis

Section 1 Experiment setup

In a situation where the valve is controlled in real water, unlike the ground, there are some unpredictable error factors such as buoyancy and clamping angle errors. In order to show that the theory is effective in real situations, experiments were conducted using robots and test benches used in previous studies. The test bench is equipped with a pipe using a suction device on the wall of the glass tank, and a valve is located in the center of the pipe. If the valve is in the water for a long period of time, the valve used in this experiment also generated a lot of rust. It increases the friction of the valve rotation operation, which became an error factor of the valve operation.

The process of the experiment is largely divided into robot submersion, assembly, setting, clamping, and operation execution. First, robots are put into a water tank, and a manipulator and a body are assembled. After moving the assembled robot to the control position, the robot is prepared as the first posture of the valve operation, and the frictional Dahl model is initialized by slightly operating the motor of the joint. And activate the gripper's pneumatic switch for clamping the valve of the manipulator. At this time, the torque sensor value is set to 0, and then the operation of rotating the valve 90 degrees clockwise is performed. Record the values of angle, torque, etc. during 90-degree rotation, and compare the values at this time to prove the effectiveness of this algorithm.

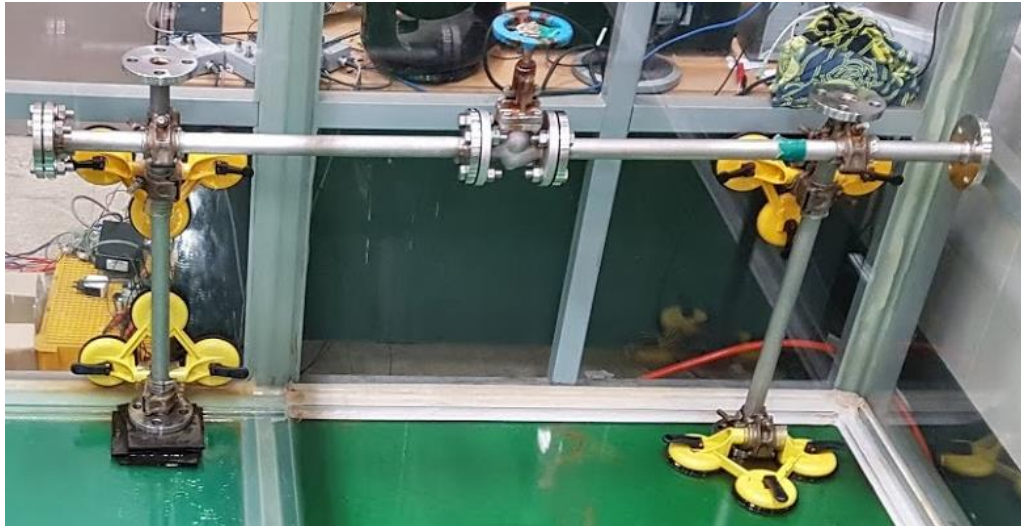


Fig. 30 Test bench and valve structures

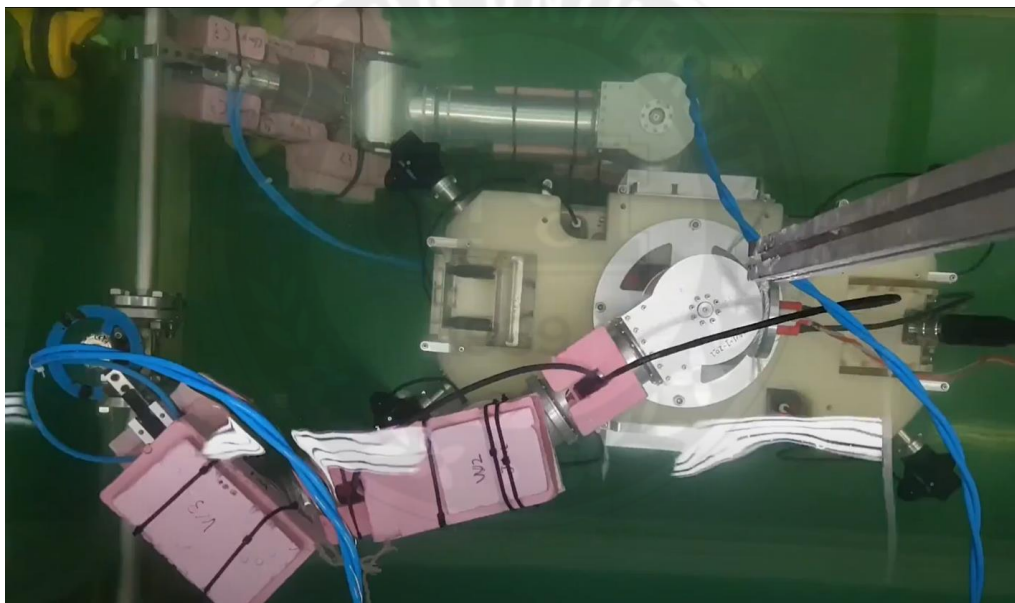


Fig. 31 AURORA – UVMS in actual experiment

Section 2 Results of Previous Study Using Weighted Matrix

The experiment was repeated two types of experiments. First, a valve work experiments were about a fixed weighting matrix used in the previous study. The other experiments were changing the weighting matrix in real time with the algorithm for minimizing the sum of squares presented in the main research topic.

In the case of using the weighting matrix used in the previous study, since the weighting matrix is fixed, the results of the iterative experiment appear similarly. Therefore, we averaged the results of iterative experiments and summarized them to compare with the changes in the algorithm. In the case of the algorithm for minimizing the sum of squares, the weighting matrix is changed each time according to error factors that are different for each experiment, so that the torque value is different each time. Therefore, we selected 3 cases (best (smallest value case), the worst (largest value case), and the average torque cases of the experiments) and compared.

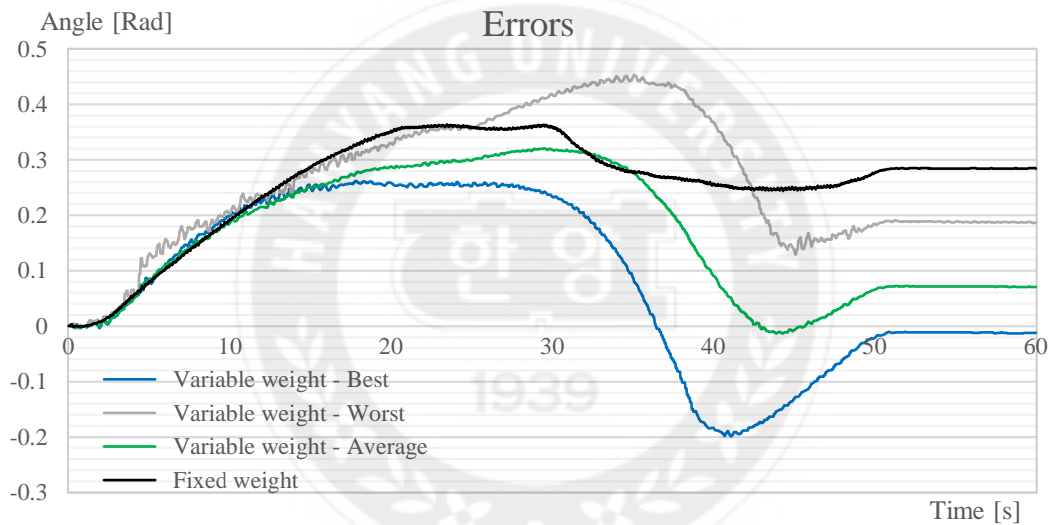


Fig. 32 The error value for the valve angle and actual rotation angle

Table 12 Error value after operation in each case				
[Rad]	Best	Worst	Average	Fixed
Error	0.012 Rad	0.186 Rad	0.070 Rad	0.284 Rad

First, since the main purpose of the experiment is to rotate the valve 90 degrees, we compared the error of the rotation angle of the valve to see if the rotation operation has been successfully performed. When comparing the error value of the actual valve rotation angle, it can be seen that the result is less error than the fixed constant. That is, it can be said that the work accuracy is higher than that of the fixed weighting matrix.

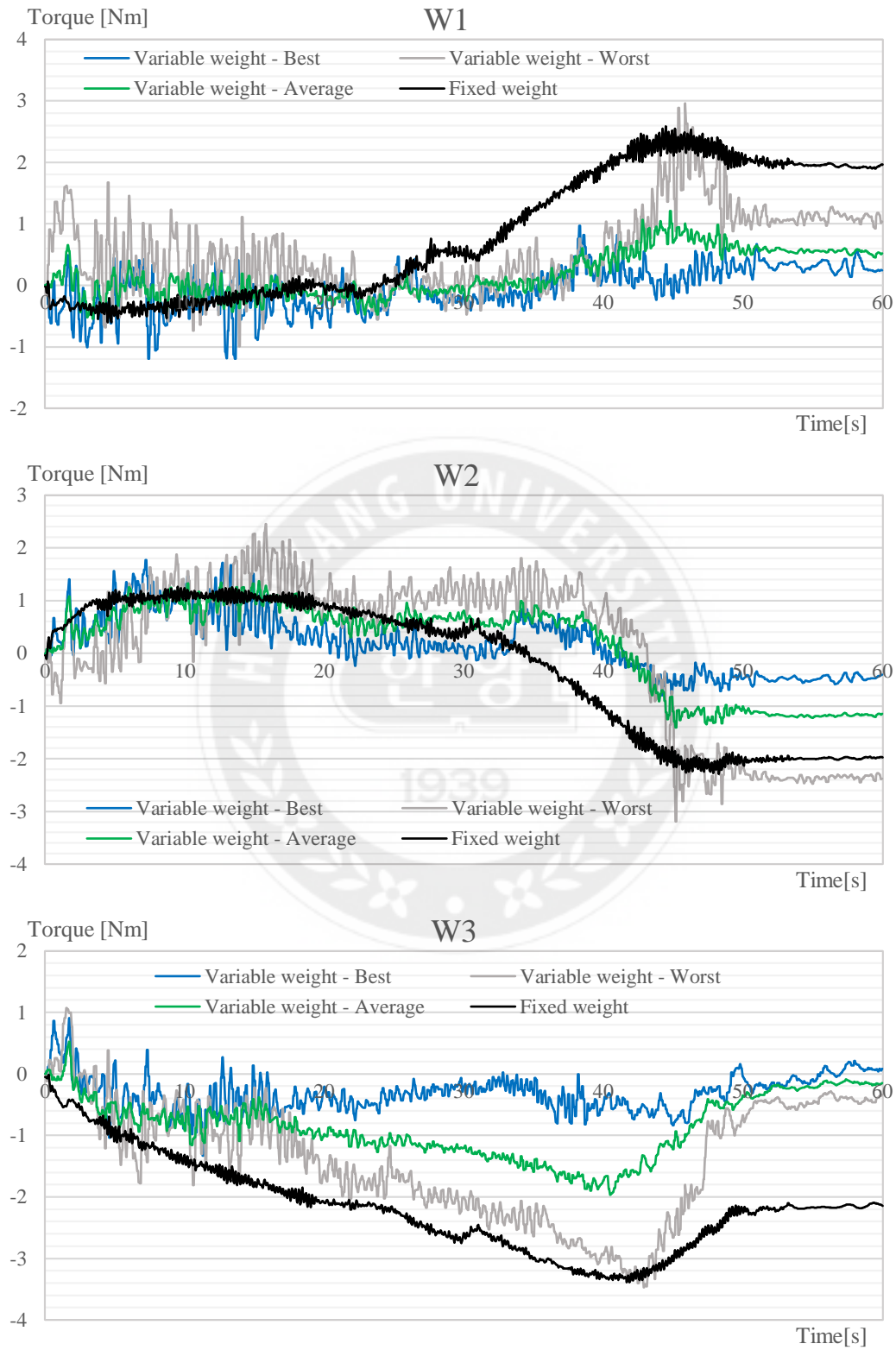


Fig. 33 Torque change of working manipulator joint W1~3 over time

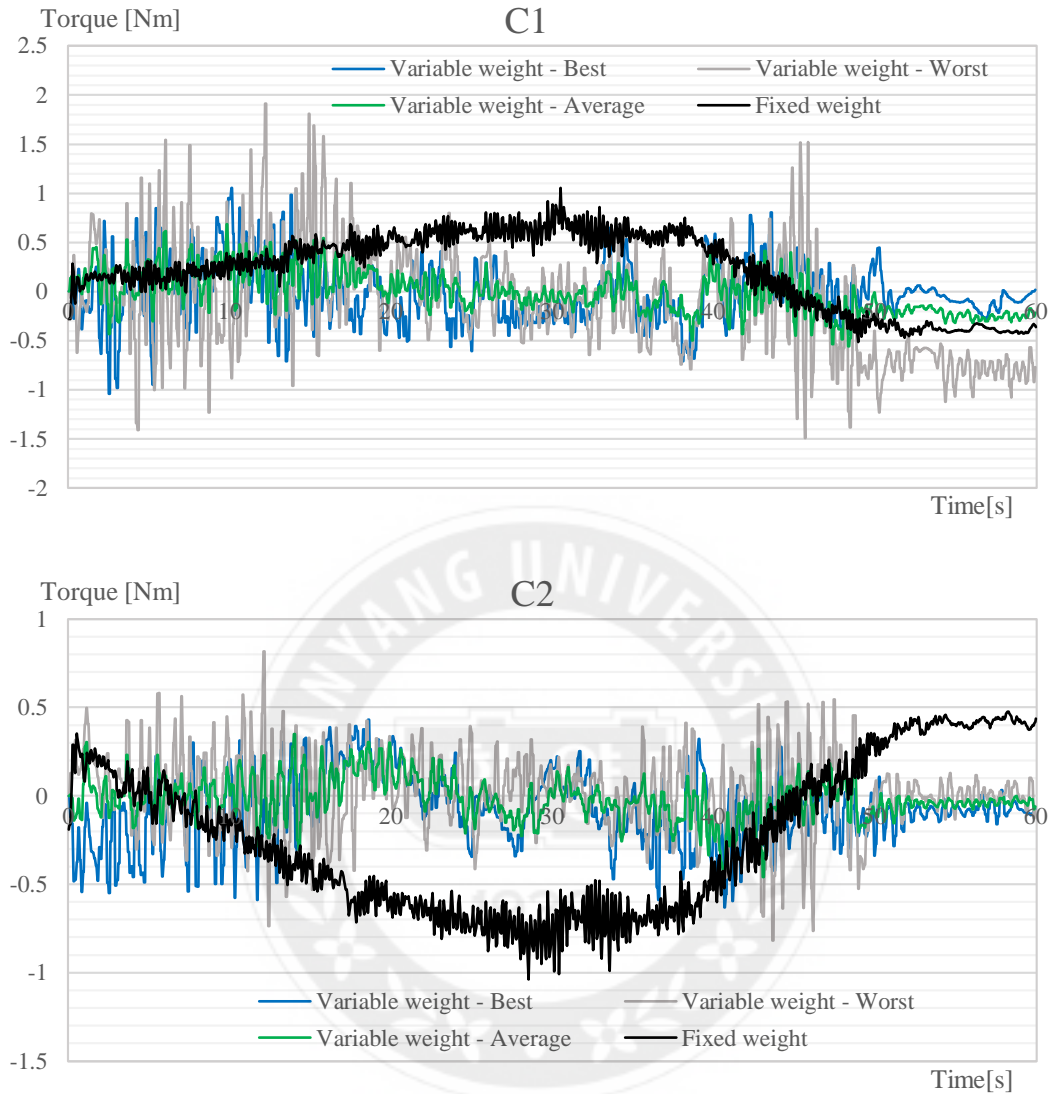


Fig. 34 Torque change of working manipulator joint C1~2 over time

Next, the torque applied to each joint is compared by using a torque sensor built into the joint. Overall, it can be seen that the torque applied during valve operation is in a decreasing trend. In the worst case, torque value sometimes becomes larger than the torque value of the matrix fixed case. However, it can be seen that the magnitude of the torque decreases overall in comparison with the matrix fixed case.

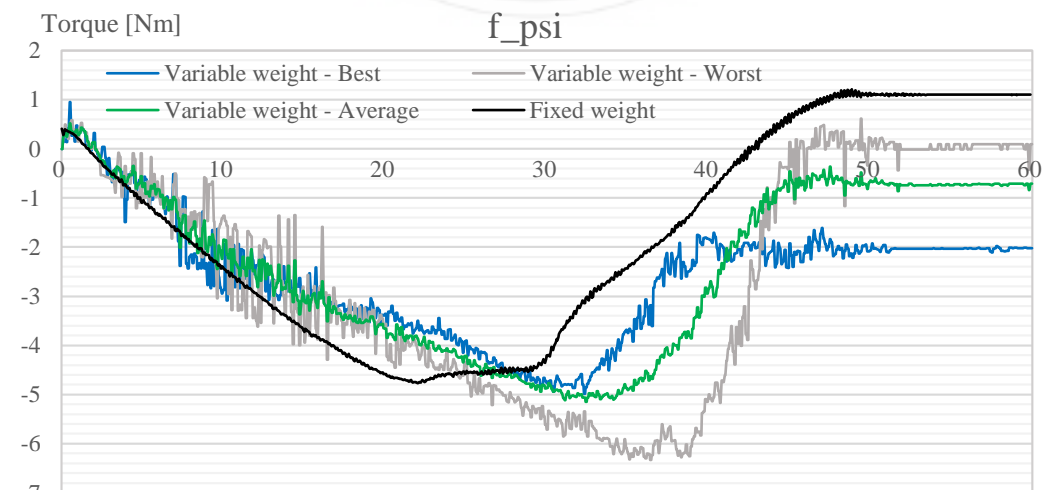
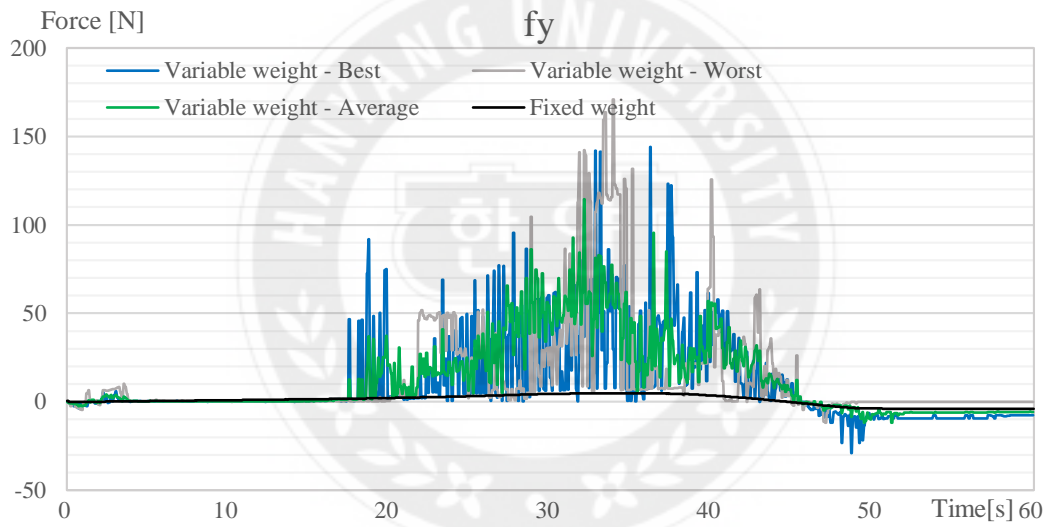


Fig. 35 Changes in the force and rotational torque of the AURORA body over time

Instead of reducing the overall torque value of the joint, the thruster's force increases significantly. In other words, it can be said that the thruster is taking over the burden on the joints. Also, when calculating the thrust limit of each thruster, each F_x, F_y can work up to 145.6N, indicating that it works well within the thrust range. For comparison, the results of the experiment are summarized as follows:

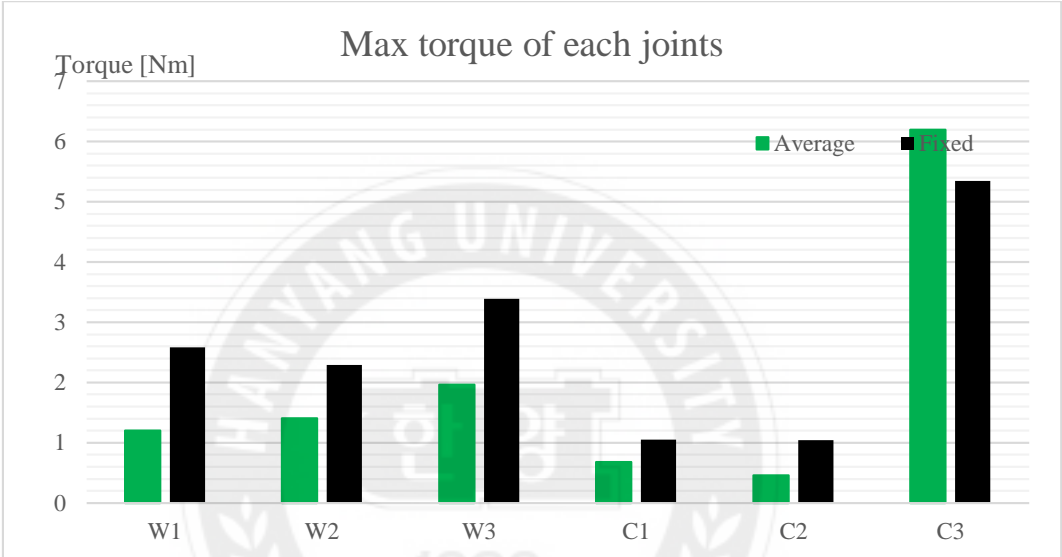


Fig. 36 Comparison of the maximum torque applied to the joint during valve operation

Table 13 Comparison of the average of the real-time Taguchi weighting matrix determination algorithm and the maximum torque of each joint in the case of a fixed constant

	W1	W2	W3	C1	C2
Average	↓ 1.4Nm	↓ 0.9Nm	↓ 1.4Nm	↓ 0.4Nm	↓ 0.6Nm
%	↓ 53 %	↓ 38 %	↓ 42 %	↓ 35 %	↓ 55 %

Table 14 Comparison difference of the maximum force and torque applied to the robot body in the case of the average and fixed constants of a real-time Taguchi weighting matrix determination algorithm

	F_x	F_y	F_ψ
Average	↑ 21.3N	↑ 109.7N	↑ 0.37N
%	↑ 114.9%	↑ 2268.3 %	↑ 7.9 %

Summarizing the results, it can be seen that the thruster can reduce the joint torque by 35 to 55% within the thrust limit.

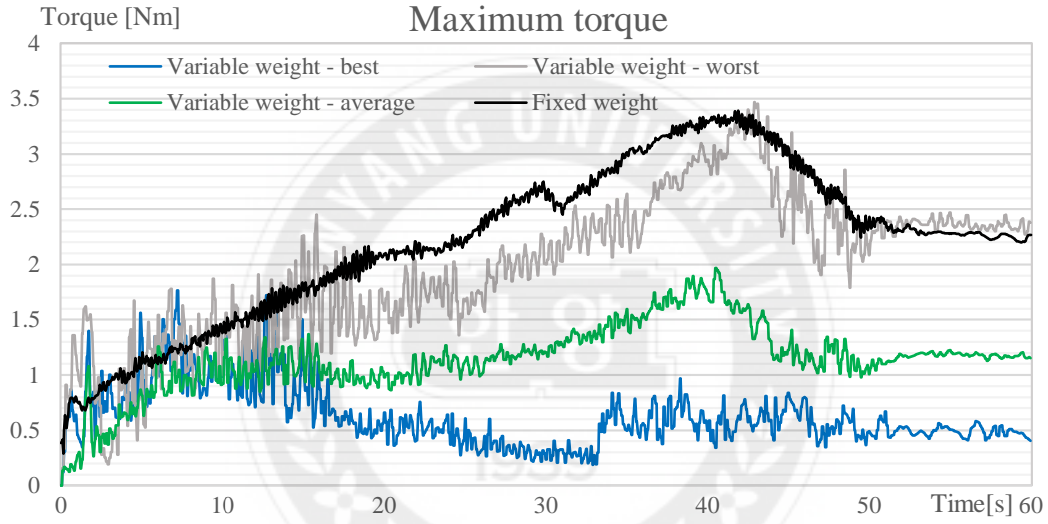


Fig. 37 Change of maximum value among manipulator joints over time

Table 15 Torque increase/decrease value compared to fixed constant when the result of the algorithm is highest, worst, or average

%	W1	W2	W3	C1	C2
Best	↓ 53.6 %	↓ 22.8 %	↓ 60.8 %	↑ 0.08 %	↓ 39.3 %
Worst	↑ 14.7 %	↑ 39.4 %	↑ 2.3 %	↑ 81.6 %	↓ 21.1 %
Average	↓ 53.3 %	↓ 38.5 %	↓ 42.0 %	↓ 35.1 %	↓ 55.8 %

To compare performance more intuitively, we compare the maximum torque size of each joint. Sometimes the maximum torque does not decrease, but it can be judged that the algorithm is useful because the torque value is generally significantly reduced due to the change in the average value.

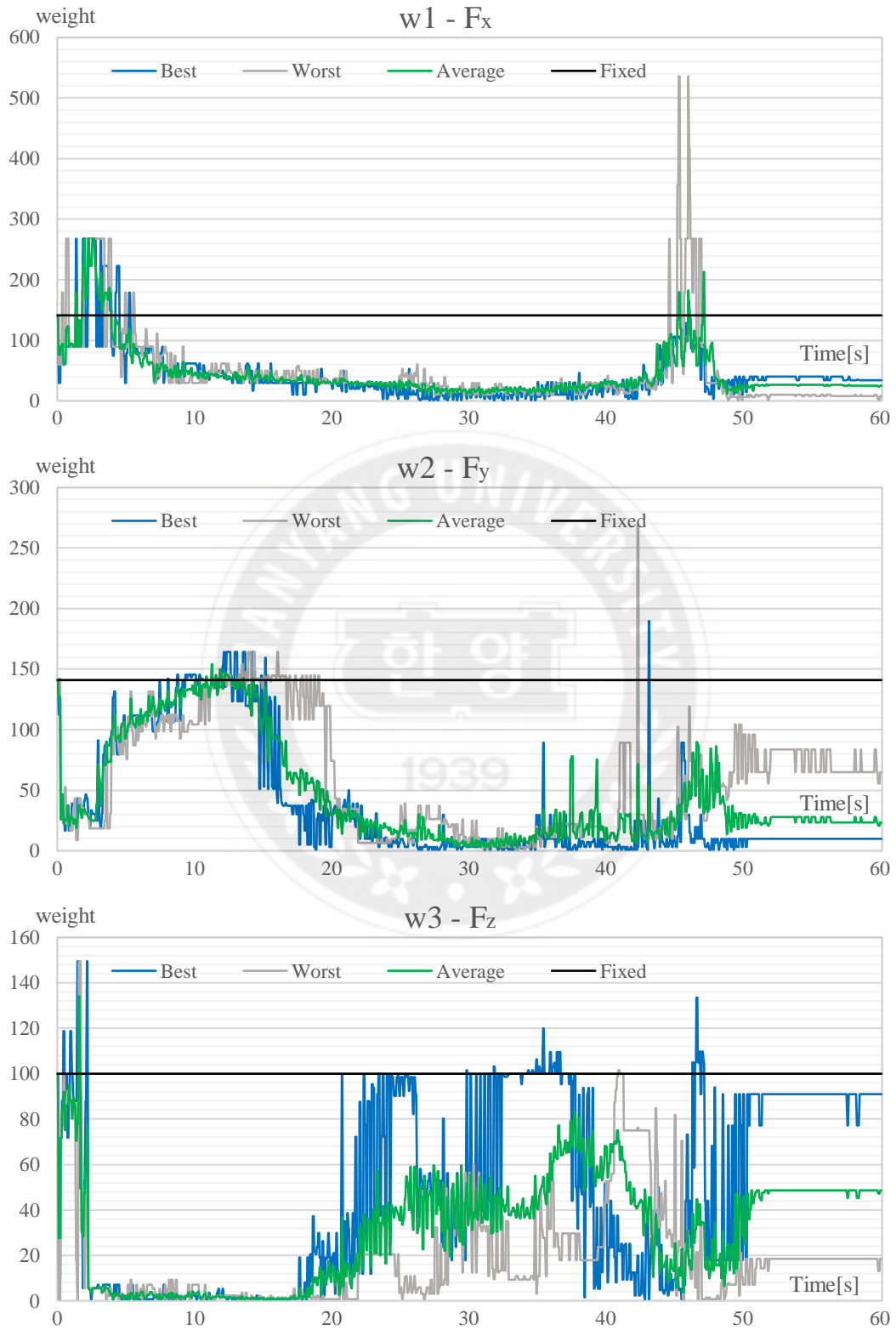


Fig. 38 Change over time of weighted matrix elements $w1 \sim w3$

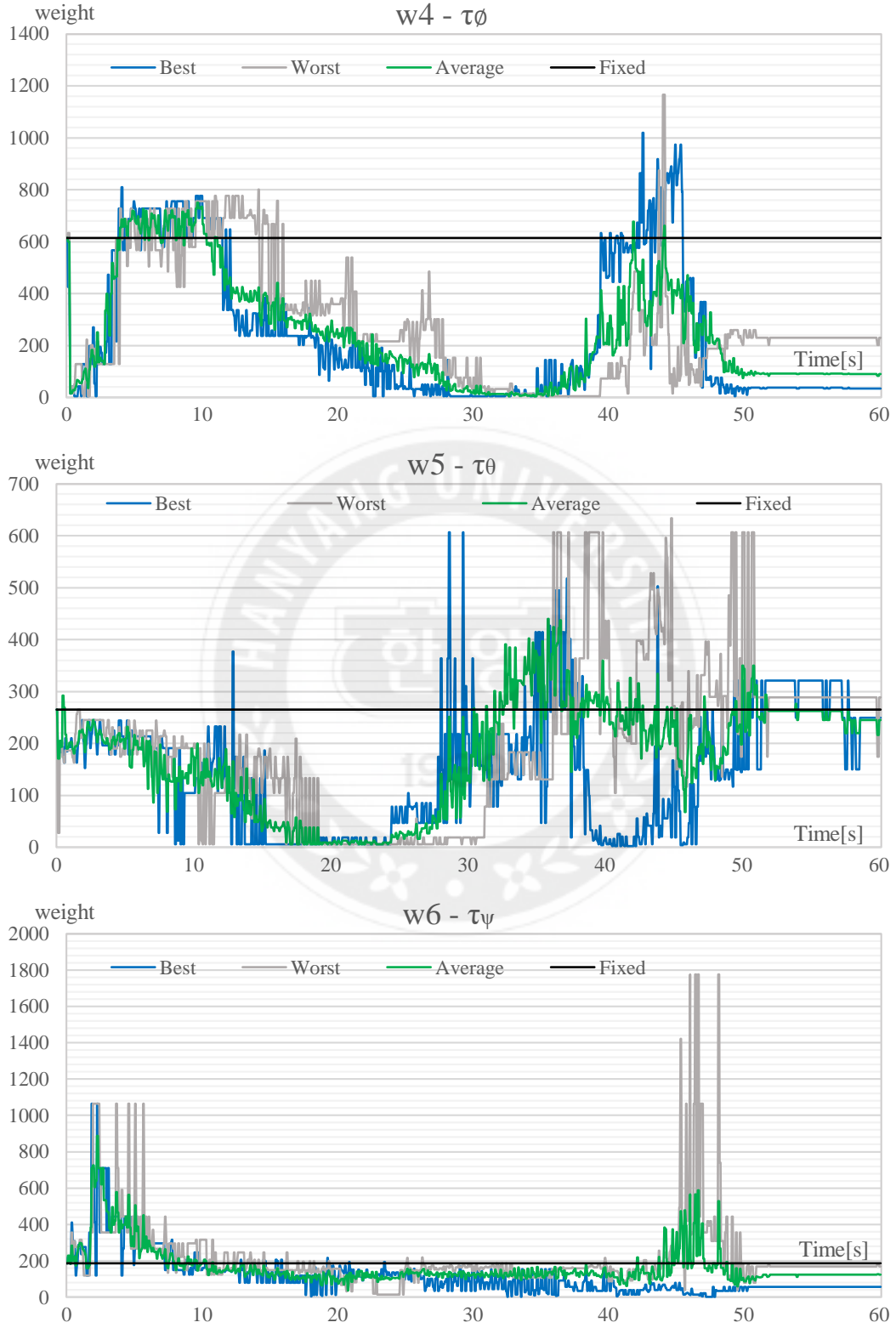


Fig. 39 Change over time of weighted matrix elements $w_4 \sim w_6$

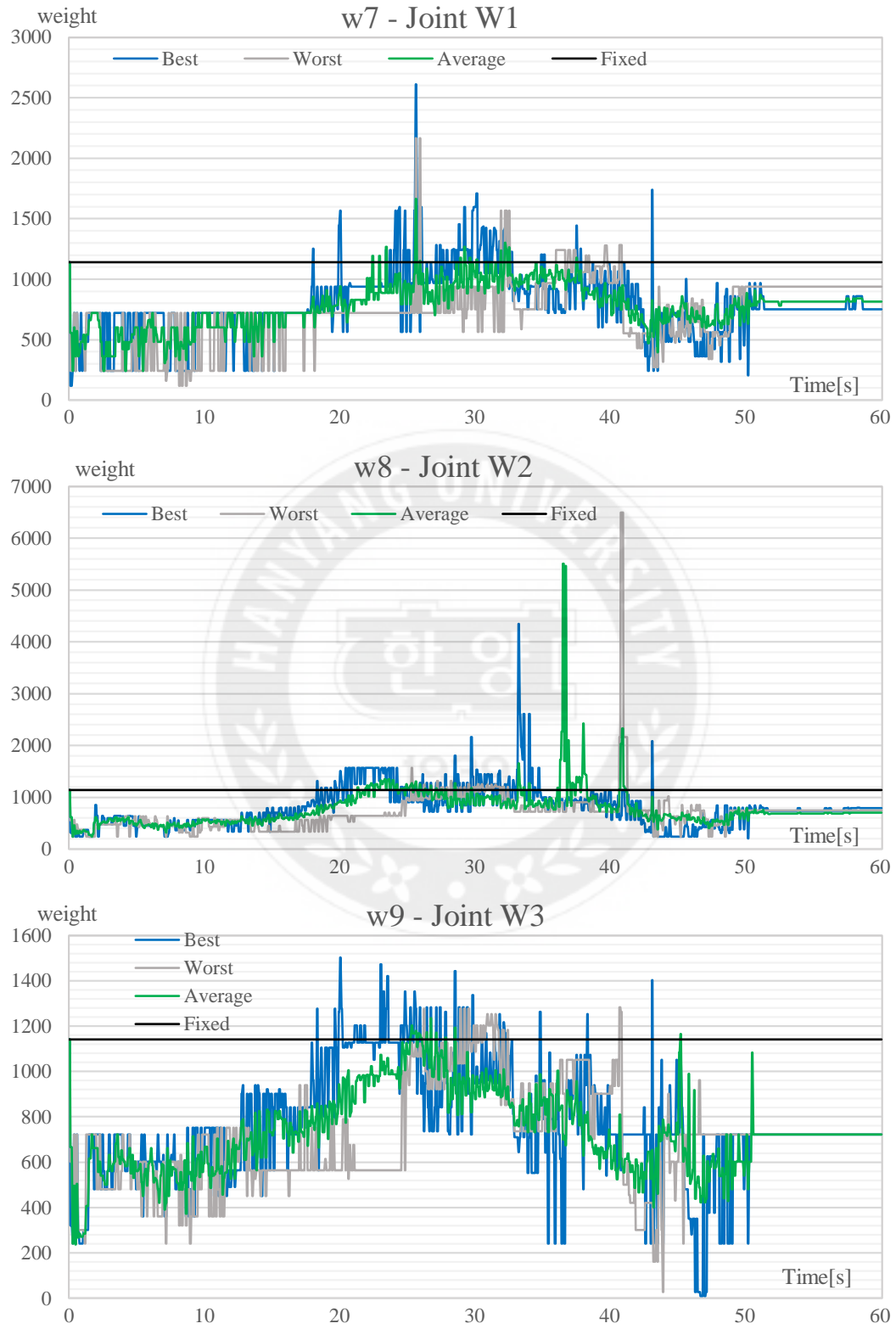


Fig. 40 Change over time of weighted matrix elements $w7 \sim w9$

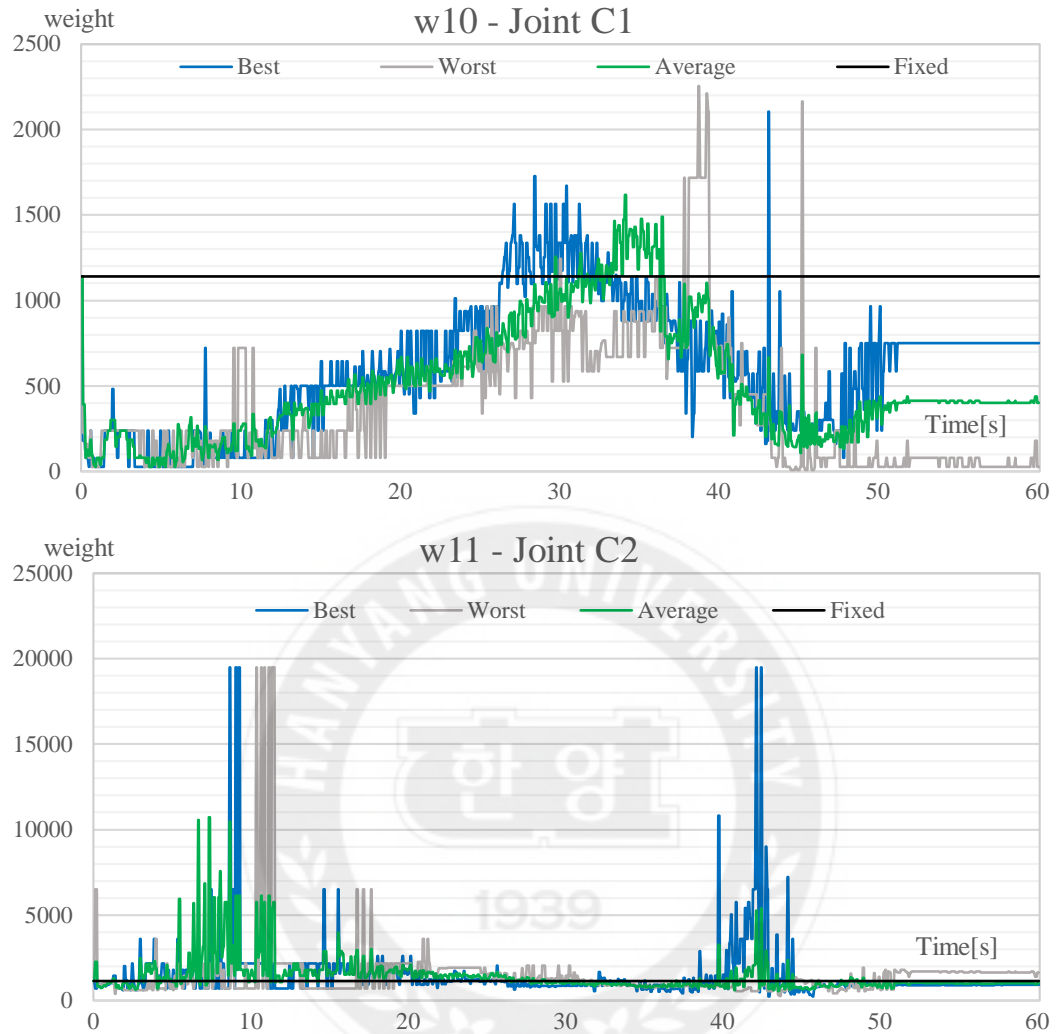


Fig. 41 Change over time of weighted matrix elements $w_{10} \sim w_{11}$

Also, when we see the change of the element values of the weighting matrix, it can be confirmed that the weighting matrix element can be adjusted in various ranges from 0 to 6500 in real time even within a limited time of the algorithm.

Chapter 5 Conclusion

In this paper, we proposed an algorithm for determining the weighting matrix that can be used for the control of a pair of manipulators attached to the AUV, which was conducted in the previous study. Previous studies have shown that the force applied to the manipulator torque can be reduced by distributing the force of the thruster and manipulator of the robot body. However, it was not suggested how to set the distribution. The method of distribution was difficult to suggest because of the many weighted matrix elements (12) and many unpredictable factors such as disturbance in the underwater situation, the clamping angle error, and obstacles. In this study, we suggest the new algorithm that can reduce torque by minimizing the sum of squared torques using the Taguchi method which can evaluate the performance and reduce the number of experiments. Then, in the actual experiment, an underwater valve experiment was conducted to compare the results. As a result, we show the algorithm is effective because the maximum value and overall burden of the actual torque is reduced.

Another contribution of this study is that the basic fundamental was prepared by changing the objective function and applying various criteria of torque distribution. In this study, the minimum of the sum of squared torques was suggested as the standard, but it can be easily changed and applied to other criteria such as the minimization of the maximum torque value in future studies. If future studies have been accumulated, the development of an auxiliary system that makes the valve work easier can be expected later.

Reference

- [1] "Annual refined petroleum products consumption - EIA," U.S Energy Information Administration (EIA), [Online]. Available: <https://www.eia.gov/international/data/world/petroleum-and-other-liquids/annual-refined-petroleum-products-consumption>. [Accessed 21 6 2020].
- [2] A. M. Tahir and J. Iqbal, "Underwater robotic vehicles: Latest development trends and potential challenges," *Science International*, vol. 26, no. 3, p. 1111–1117, 2014.
- [3] G. Ho, N. Pavlovic and R. Arrabito, "Human factors issues with operating unmanned underwater vehicles," *Proceedings of the Human Factors and Ergonomics Society Annual Meeting*, pp. 429–433, 2011.
- [4] I. Lemaire, "NOSC and Remotely Operated Vehicles (ROVs) and Autonomous Unmanned Vehicles (AUVs)," Naval Ocean Systems Center, San Diego, 1988.
- [5] R. D. Christ and R. L. W. Sr., *The ROV Manual: A User Guide to Observation-class Remotely Operated Vehicles*, Burlington: Elsevier, 2007.
- [6] J. Yuh, "Design and control of autonomous underwater robots: A survey," *Autonomous Robots*, vol. 8, no. 1, pp. 7–24, 2000.
- [7] S. Sivčev, J. Coleman, E. Omerdić, G. Dooly and D. Toal, "Underwater manipulators: A review," *Ocean Engineering*, vol. 163, pp. 431–450, 2018.
- [8] M. Pittelkau, "Adaptive load-sharing force control for two-arm manipulators," *Proceedings. 1988 IEEE International Conference on Robotics and Automation*, pp. 498–503, 1988.
- [9] K. Koyanagi, H. Hirukawa, S. Hattori, M. Morisawa, S. I. Nakaoka, K. Harada and S. Kajita, "A pattern generator of humanoid robots walking on a rough terrain using a handrail," *2008 IEEE/RSJ International Conference on Intelligent Robots and Systems*, pp. 2617–2622, 2008.
- [10] Y. Seki, S. Sagara and R. Ambar, "Impedance Control of Dual-Arm 3-link Underwater Robot: In the Case of Grasping a Fixed Object Lightly with One Hand," *2018 International Conference on Information and Communication Technology Robotics (ICT-ROBOT). IEEE*, pp. 1–4, 2018.
- [11] J. Bae, *Cooperative operation of underwater robotic vehicle and dual-arm manipulator*, Seoul National University: PhD diss., 2019.
- [12] S. Jin, *Hovering Control of an Underwater Robot with Tilting Thrusters Enabling Various Works*, Seoul National University: PhD diss, 2014.
- [13] J. Bak, *Optimal hovering control of an underwater robot with redundant tilting thrusters*, Seoul National University: PhD diss., 2020.
- [14] C. Pickover, *Archimedes to Hawking: laws of science and the great minds behind them*, Oxford University Press, 2008.
- [15] P. R. Dahl, "A solid friction model," *The Aerospace Corporation*, El Segundo, 1968..
- [16] H. Olsson, K. J. Åström, C. C. De Wit, M. Gäfvert and P. Lischinsky, "Friction Models and Friction Compensation," *European Journal of Control*, vol. 4, no. 3, pp. 176–195, 1998.
- [17] S. Lee, *Research on antagonistic stiffness for over-actuated parallel mechanisms*, Seoul National University: PhD diss., 2008.
- [18] I. Schjølberg and T. . Fossen, "Modelling and control of underwater vehicle-manipulator systems," *Proc. rd Conf. on Marine Craft maneuvering and control*, p. 45–57, 1994.

- [19] H. Cheng, Y.-K. Yiu and Z. Li, "Dynamics and control of redundantly actuated parallel manipulators," *IEEE/ASME Transactions on mechatronics*, vol. 8, no. 4, pp. 483-491, 2003.
- [20] B. J. Yum, S. J. Kim, S. K. Seo, J. H. Byun and S. H. Lee, "The Taguchi robust design method: Current status and future directions," *Journal of Korean Institute of Industrial Engineers*, vol. 39, no. 55, pp. 325-341, 2013.
- [21] G. S. Peace, *Taguchi Methods: A Hands-on Approach to Quality Engineering*, Addison-Wesley, 1993.
- [22] N. K. Sharma and E. A. Cudney, "Signal-to-Noise ratio and design complexity based on Unified Loss Function–LTB case with Finite Target," *International Journal of Engineering*, vol. 3, no. 7, pp. 15-24, 2011.
- [23] G. Antonelli, "Underwater Robots," *Springer Tracts in Advanced Robotics*, vol. 96, 2014.
- [24] J. Yuh and M. West, "Underwater robotics. Adv. Robot.," *Advanced Robotics*, vol. 15, no. 5, p. 609–639, 2001.
- [25] S. Jin, J. Kim, J. Kim and T. Seo, "Six-degree-of-freedom hovering control of an underwater robotic platform with four tilting thrusters via selective switching control," *IEEE/ASME Transactions on*, vol. 20, no. 5, pp. 2370-2378, 2015.
- [26] L. Eldén, "A weighted pseudoinverse, generalized singular values, and constrained least square problems," *BIT Numerical Mathematics*, vol. 22, no. 4, pp. 487-502, 1982.



Appendix

Summary of equation variable

\mathbf{v}	$[\mathbf{u}, \mathbf{v}, \mathbf{w}, \mathbf{p}, \mathbf{q}, \mathbf{r}]^T$
\mathbf{M}_v	Inertia matrix with added mass terms of the vehicle
$\mathbf{C}_v(\mathbf{v})$	The centrifugal and Coriolis force matrix
$\mathbf{D}_v(\mathbf{v})$	The hydrodynamic drag matrix
\mathbf{g}_v	Gravity as well as buoyancy vector
$\boldsymbol{\tau}_v$	The thrust force vector of the vehicle
\mathbf{q}	The manipulator joint angle vector
$\boldsymbol{\tau}_m$	The manipulator joint torque
\mathbf{v}	Vehicle
\mathbf{w}	Working manipulator
\mathbf{c}	Clamping manipulator
\mathbf{M}	Represents the inertia matrix including added mass terms,
\mathbf{D}	Represents the hydrodynamic drag.
\mathbf{H}	Denotes inertia added from a manipulator to the vehicle
\mathbf{M}_c	The reaction force and moment induced between a manipulator and vehicle
\mathbf{D}_i	Quadratic drag terms caused by interactions between the vehicle and manipulators
$\boldsymbol{\tau}$	$[\boldsymbol{\tau}_v^T, \boldsymbol{\tau}_w^T, \boldsymbol{\tau}_c^T]^T$. The drive force and torque vector, which comprises vehicle thrust force and joint torques of the two manipulators
\mathbf{W}	$\text{diag}(w_x, w_y, w_z, w_\phi, w_\theta, w_\psi, w_{w1}, w_{w2}, w_{w3}, w_{c1}, w_{c2}, w_{c3})$. Weighting matrix
$(\boldsymbol{\Gamma}^T)^\#$	Weighted pseudoinverse of transposed constraint Jacobian matrix
\mathbf{e}	$q_{u,d} - q_u$. error vector of the independent joint angles
\mathbf{W}_d	$\text{diag}(w_x, w_y, w_z, w_\phi, w_\theta, w_\psi, w_{w1}, w_{w2}, w_{w3}, w_{c1}, w_{c2}, w_{c3})$. Adjusting weighting matrix
\mathbf{f}_d	Disturbance force applied on the vehicle
\mathbf{J}_b	Jacobian matrix between the independent joints and the vehicle position and orientation
$\boldsymbol{\tau}_{r.desired}$	The actuated joint torque

국문 요지

해저에는 다양한 활용 가능성이 있는 자원이 잠들어 있고, 이를 활용하기 위해서 다양한 수중 로봇 기술이 발달해 왔다. 그 중에서 석유와 가스 채굴에 관련되어 많이 사용되는 수중 밸브 제어 기술 역시 많이 연구되어 왔다. 그래서 이전 연구에서는 수중 로봇과 매니퓰레이터를 이용한 수중 밸브 회전 작업 중에 본체에 관절의 부담을 분배하여 관절의 토크 부담을 낮추는 연구가 진행되었다. 그러나 이 연구에는 그 분배를 어떻게 해야 더 관절의 부담을 감소 시킬 수 있을지에 대해서는 다루지 않았다. 본 연구에서는 다구치 방법론을 통해 센서 값 기반으로 가중 행렬을 결정하여, 변하는 환경에 대응하여 관절의 토크를 감소시킬 수 있는 새 알고리즘을 제시하였다. 그리고 이를 실제 수조에서 고정 가중 행렬의 경우와 본 연구의 알고리즘의 경우를 반복 실험을 해서 결과를 비교하였다. 그래서 기존의 고정된 가중 행렬로 밸브 작업을 진행하는 것 보다 매니퓰레이터 관절의 최대 토크를 35~55% 더 낮아지는 것을 관찰하여 본 알고리즘의 효용성을 입증하였다.

연구 윤리 서약서

본인은 한양대학교 대학원생으로서 이 학위논문 작성 과정에서 다음과 같이 연구 윤리의 기본 원칙을 준수하였음을 서약합니다.

첫째, 지도교수의 지도를 받아 정직하고 엄정한 연구를 수행하여 학위논문을 작성한다.

둘째, 논문 작성시 위조, 변조, 표절 등 학문적 진실성을 훼손하는 어떤 연구 부정행위도 하지 않는다.

셋째, 논문 작성시 논문유사도 검증시스템 "카피킬러"등을 거쳐야 한다.

2020년06월19일

학위명 : 석사

학과 : 융합기계공학과

지도교수 : 서태원

성명 : 문예철



한 양 대 학 교 대 학 원 장 귀 하

Declaration of Ethical Conduct in Research

I, as a graduate student of Hanyang University, hereby declare that I have abided by the following Code of Research Ethics while writing this dissertation thesis, during my degree program.

"First, I have strived to be honest in my conduct, to produce valid and reliable research conforming with the guidance of my thesis supervisor, and I affirm that my thesis contains honest, fair and reasonable conclusions based on my own careful research under the guidance of my thesis supervisor.

Second, I have not committed any acts that may discredit or damage the credibility of my research. These include, but are not limited to : falsification, distortion of research findings or plagiarism.

Third, I need to go through with Copykiller Program(Internet-based Plagiarism-prevention service) before submitting a thesis."

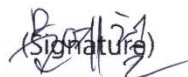
JUNE 19, 2020

Degree : Master

Department : DEPARTMENT OF MECHANICAL CONVERGENCE ENGINEERING

Thesis Supervisor : SEO, TAEWON

Name : MOON YE CHEOL


(Signature)